Chemical Engineering Journal 540 (2026) 177409

Contents lists available at ScienceDirect

Chemical Engineering Journal

journal homepage: www.elsevier.com/locate/cej

Impact of brominated flame retardants on the chemical recycling of polystyrene via pyrolysis

Razan Alsharqawi [a], Daniela Merz [a], Tim Kurtz [a], Michael Zeller [a], Niklas Netsch [a], Britta Bergfeldt [a], Salar Tavakkol [a,*], Dieter Stapf [a]

[a] Institute for Technical Chemistry (ITC), Karlsruhe Institute of Technology (KIT), Herrmann-von-Helmholtz-Platz 1, 76344 Eggenstein-Leopoldshafen, Germany

ARTICLE INFO

Keywords:
Pyrolysis
Polystyrene
ETICS
PolyFR
HBCD
Brominated flame retardants

ABSTRACT

Brominated flame retardants remain a key challenge for the chemical recycling of polystyrene, particularly for expanded polystyrene used in external thermal insulation composite systems. Pyrolysis offers a viable route to recover monomer-rich oils, provided that bromine can be efficiently separated. In this study, the pyrolysis behavior of flame-retarded polystyrene containing hexabromocyclododecane and brominated butadiene-styrene-copolymer is investigated with a focus on bromine release and product composition. Thermogravimetric analysis coupled with Fourier-transform infrared spectroscopy shows that approximately 90 wt% of bromine is released as hydrogen bromide below 350 °C, largely independent of composition. At elevated flame-retardant contents, stabilization effects emerge at higher temperatures due to interactions between flame-retardant decomposition intermediates and the polystyrene matrix. Pyrolysis-gas chromatography–mass spectrometry indicates that, at application-relevant loadings, the styrene-dominated product distribution remains unchanged. Heating rate variation reveals temporal separation between dehydrobromination and PS depolymerization, with rapid bromine release occurring under conditions relevant to technical pyrolysis. These findings demonstrate that pyrolysis can effectively direct bromine to the gas phase without compromising product quality, providing a basis for temperature-driven process design and advancing circular recycling strategies for flame-retarded polystyrene waste.

1. Introduction

The transition to a circular economy is a central component of Europe's strategy for sustainable development and climate neutrality by 2050 [1,2]. In this context, waste management increasingly prioritizes preserving material value and closing resource loops through reuse, remanufacturing, and recycling across the product life cycle [3].

Approximately 88% of expanded polystyrene (EPS) waste originating from external thermal insulation composite systems (ETICS) generated in Germany was incinerated in 2021 [4]. Although absolute volumes are relatively low, municipal solid waste incineration plants are already operating near maximum capacity. Moreover, the high calorific value of EPS presents technical challenges during combustion, even at current waste levels [5]. While incineration enables energy recovery, it disregards the potential for material recycling and therefore limits progress toward circularity. EPS waste from ETICS is expected to increase substantially over the coming decades. With a typical service life of 40–60 years [4], many ETICS installations are approaching their end-of-life phase. Projections suggest that EPS waste volumes will double by 2030 [3] and quadruple by 2050 [5], highlighting the need for scalable alternatives to incineration.

A major barrier to recycling EPS insulation is its flame-retardant content [6]. For decades, hexabromocyclododecane (HBCD) was the standard additive flame retardant used for fire safety purposes in polystyrene (PS) insulation materials [4] (meaning it is not covalently bound to the polymer matrix). HBCD is an aliphatic brominated flame retardant (BFR) containing 71–75 wt% bromine [7]. The chemical structure of HBCD ($C_{12}H_{18}Br_6$) is shown in Fig. 1. Due to its persistence, bioaccumulation, and toxicity, HBCD was listed under the Stockholm Convention on Persistent Organic Pollutants (POPs) in 2013 [8], and its manufacture and use have been banned across Europe since 2016 [9]. Although HBCD loadings in EPS insulation typically did not exceed 2 wt% [8,10], the mechanical recycling of this material is prohibited because the additive is not removed during processing, and could therefore be

* Corresponding author.
E-mail address: salar.tavakkol@kit.edu (S. Tavakkol).

https://doi.org/10.1016/j.cej.2026.177409
Received 23 March 2026; Received in revised form 3 May 2026; Accepted 14 May 2026
Available online 18 May 2026

reintroduced into the environment [4]. Owing to the long service life of building insulation, HBCD-containing EPS will continue to enter the waste stream for decades, thereby limiting mechanical recycling options far into the future.

To replace HBCD, a polymeric flame retardant known as PolyFR was developed [11]. PolyFR is a brominated styrene-butadiene-styrene triblock copolymer that is selectively brominated at the 1,2- and 1,4-isomeric units of the butadiene block, as shown in Fig. 2. Incorporation of styrene units into the flame retardant's backbone improves thermal stability and compatibility with PS in blend formulations [12]. PolyFR is an additive BFR that contains approximately 64 wt% bromine. Because bromine is bound to the aliphatic butadiene block, PolyFR is classified as an aliphatic flame retardant [13]. Due to its higher molecular weight (> 100,000 Da vs. 642 Da for HBCD [14,15]), PolyFR exhibits a lower tendency to migrate from PS insulation materials and is therefore considered to have a reduced environmental impact compared to HBCD [11,16]. In PS blends, PolyFR provides flame retardancy through similar gas-phase and condensed-phase mechanisms as HBCD, releasing bromine radicals and promoting polymer decomposition [7,9,12]. Since 2016, PolyFR has been the standard flame retardant used in newly produced flame-retarded EPS in Western countries [4,10]. Because long term behavior of PolyFR is still unknown [15,17], it is not classified as a hazardous substance. Hence, its potential entry into recycling streams for packaging EPS cannot be excluded [18,19]. Consequently, current end-of-life management still relies on incineration, highlighting the need for alternatives.

In this context, pyrolysis has gained increasing attention as a promising chemical recycling route for polymers [20–22], including PS-based materials [3,5,23,24]. During pyrolysis, polymers are thermally decomposed into smaller molecules at temperatures above 300 °C in an inert atmosphere [20]. EPS decomposes predominantly into styrene monomer and oligomers, yielding a monomer-rich oil that can serve as a secondary raw material for circular PS production [3,20,23]. The underlying decomposition chemistry follows the well-established radical chain scission mechanism of PS $(C_8H_8)_n$, involving initiation, propagation, and termination reactions [25]. Initiation occurs via random backbone scission to form macroradicals. Propagation proceeds through three main pathways: (i) unzipping, the dominant route for styrene formation, (ii) intermolecular hydrogen transfer followed by mid-chain β-scission [11,26], producing low-molecular-weight fragments and macroradicals [27], and (iii) intramolecular hydrogen transfer followed by mid-chain β-scission [26,27], generating styrene dimer and trimer via 1,3- and 1,5-hydrogen transfer, respectively [27]. Thermogravimetric analysis (TGA) shows that the expansion of PS into EPS has minor influence on the thermal decomposition behavior [11]. In nitrogen and at 10 K•min^{-1}, both materials decompose in a single step from 325 to 450 °C, leaving no solid residue [28,29].

Despite the favorable product distribution [23], the industrial applicability of pyrolysis oils from PS-based ETICS waste is constrained by stringent impurity limits. PS manufacturers accept pyrolysis oils only when contaminant levels are sufficiently low [20]. Although no bromine specification has been published for circular PS feedstock, halogen tolerance is generally expected to be very low due to well-known issues such as corrosion, salt formation, and operational disruptions [30,31]. In the absence of dedicated limits for bromine, chlorine specifications applied in established petrochemical processes, for example 3 ppm in steam crackers [30], provide a useful reference for the level of impurity control required. For high circularity, recovered styrene must be suitable for direct reuse in PS production. Consequently, effective bromine removal is a prerequisite for both closed-loop PS recycling and for ensuring compatibility with existing polymer manufacturing infrastructure.

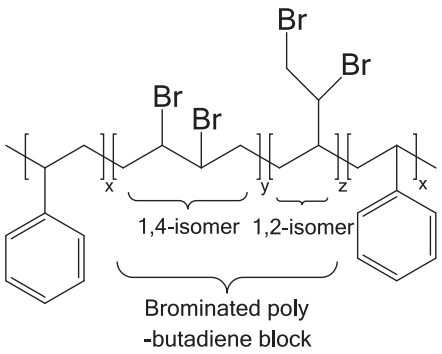

Fig. 2. Chemical structure of PolyFR, recreated as per [13].

However, the influence of BFRs used in insulation-grade EPS on PS pyrolysis remains insufficiently investigated. Existing studies have shown that HBCD-containing PS exhibits a lower decomposition onset temperature than non-flame-retarded PS [32,33]. For example, Beach et al. attributed this behavior to homolytic C—Br cleavage in HBCD, which facilitates subsequent hydrogen abstraction from the PS backbone and promotes earlier radical formation. They proposed two hydrogen abstraction pathways, both requiring lower bond dissociation energies than those involved in the initiation reaction in non-flame-retarded PS. Their qualitative analyses identified styrene as the dominant product alongside oligomers and HBr, with maximum HBr evolution occurring at approximately 290 °C and styrene release at approximately 390 °C [32].

Thermal analysis studies report that HBCD decomposes from 230 to 270 °C at 10 K•min^{-1} under nitrogen [7], largely independent of isomeric compositions (see Fig. 1), owing to the rapid establishment of isomeric equilibrium [7,33]. Decomposition proceeds via a radical-driven, autocatalytic mechanism with substantial bromine release as HBr (77–84 wt%) [7,34]. Sequential HBr elimination leads to debrominated intermediates [35,36], suggesting that bromine is predominantly transferred to the gas phase during thermal treatment.

In contrast, significantly fewer studies have addressed the thermal decomposition of PolyFR. Available literature indicates a two-step decomposition behavior involving C—Br bond cleavage at 265–320 °C, followed by slower decomposition of debrominated structures at 230–500 °C [11,12]. While these studies provide initial

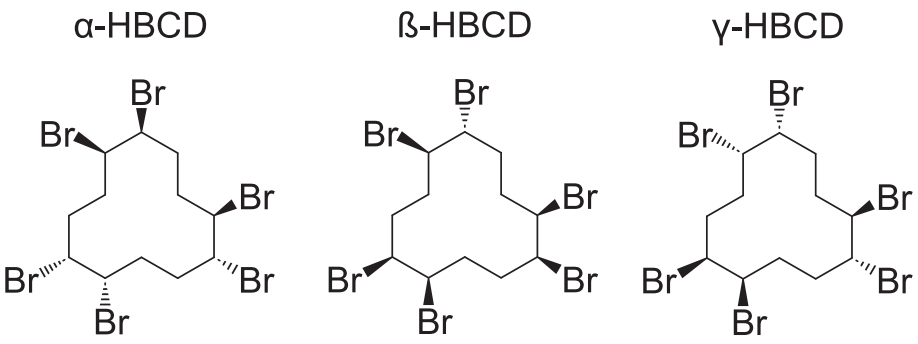

Fig. 1. Chemical structures of the α-, β-, and γ-HBCD enantiomers predominate in all technical HBCD mixtures, recreated as per [9].

mechanistic insights, they are limited to isolated PolyFR and do not consider its interaction with PS. A systematic understanding of the pyrolysis behavior of PolyFR-containing PS is therefore still lacking. To the best of our knowledge, quantitative data on HBr formation and its dependence on process conditions have not yet been reported.

Moreover, previous studies separately examine PS depolymerization [23,27], HBCD-induced decomposition shifts in PS [30,31], and the thermal behavior of PolyFR [12,16]. Investigations addressing the pyrolysis behavior of PolyFR-containing PS, as well as comparisons between the legacy HBCD and the younger PolyFR in PS pyrolysis, remain scarce. As a result, the feasibility of pyrolysis as a recycling route for flame-retarded insulation-grade EPS remains uncertain. Bridging this gap is essential to assess whether pyrolysis of flame-retarded ETICS-derived PS waste can produce bromine-poor oil fractions that are suitable for downstream use while effectively separating bromine into the gas phase.

Against this background, the present study compares the influence of HBCD and PolyFR on the pyrolysis behavior of EPS by combining thermal analysis with product characterization. A method for quantitative HBr accounting is developed and applied to PS-based model mixtures with elevated PolyFR loadings. In addition, the effect of heating rate on HBr evolution is examined. This work evaluates whether pyrolysis can yield a bromine-poor oil fraction alongside an HBr-rich gas phase and identifies the factors governing the observed thermal behavior. The resulting insights provide a foundation for pyrolysis-based recycling strategies for flame-retarded EPS from ETICS by addressing bromine contamination, a key bottleneck for high-quality circular PS production.

2. Materials and methods

2.1. Model samples

The investigated samples were chosen to represent both realistic waste streams and controlled model systems relevant to flame-retarded EPS insulation. HBCD-containing EPS was included as a legacy material commonly found in demolition waste from ETICS, while PolyFR-containing EPS represents the current industrial standard for newly produced insulation materials and a future waste stream. Non-flame-retarded EPS was used as a reference to isolate the influence of BFRs on pyrolysis behavior. This combination enables a direct comparison between legacy and replacement BFRs under application-relevant conditions.

The compositions, ash contents, as well as the higher heating values (HVV) of the real EPS samples are listed in Table 1. HBCD-containing EPS waste (EPS-HBCD), collected from demolished buildings and mechanically compacted into blocks, was provided by LANXESS AG. Commercial PolyFR-containing EPS (EPS-PolyFR) was supplied by RYGOL Dämmstoffe Werner Rygol GmbH & Co. KG, and non-flame-retarded EPS (Styropor/Airpop) was obtained from Schlaadt Plastics GmbH. Key physical properties of the investigated EPS samples are summarized in Table 2.

Table 1
Elemental compositions, ash contents, and HVV of the commercial samples.

Sample	C/wt %	H/wt %	Br/wt %	BFR loading/ wt%	Ash[d]/wt %	HHV[e]/ MJ•kg^{-1}
EPS-HBCD	92.0[a]	7.2[a]	0.2[b]	0.3[c]	0.57	40.8
EPS-PolyFR	91.7[a]	7.6[a]	0.3[b]	0.5[c]	0.31	40.5
EPS	92.0[a]	7.8[a]	–	–	0.13	41.3

[a] Determined on a dry basis using a LECO elemental analyzer (Truspec CHN Micro).
[b] Determined experimentally via combustion ion chromatography (C-IC).
[c] Calculated based on the elemental analysis.
[d] Determined in accordance with DIN EN ISO 3451-1:2008-11.
[e] Determined in accordance with DIN 51900:2023-12.

While the samples listed in Table 1 reflect realistic compositions, the low BFR loadings present an analytical limitation. At 0.2 and 0.3 wt% bromine, bromine-containing pyrolysis products are close to detection limits. To overcome this and enable a quantitative and mechanistic assessment of bromine release and bromine-related effects, model mixtures with elevated BFR loadings were prepared.

Due to regulatory restriction on the purchase and use of HBCD in the European Union [9], model mixtures with elevated HBCD loadings were not prepared. For this purpose, only PolyFR was used. Mixtures containing 25, 50, and 75 wt% PolyFR were selected to systematically increase bromine content, thereby enhancing analytical sensitivity and enabling reliable detection of HBr. These compositions do not represent application-relevant formulations but provide a controlled framework to investigate composition-dependent effects and interaction phenomena.

The model mixtures were prepared by manually mixing PS and PolyFR. Pure PolyFR was supplied by LANXESS AG. General-purpose PS granules (Styrolution PS 124N, INEOS Styrolution) were ground to 500 µm and mixed with PolyFR powder at room temperature by gentle shaking. Individual masses of PS and PolyFR controlled to within ±8 µg to ensure reproducibility. The mixtures are denoted as PSXPolyFR, where X indicates the PolyFR content in wt% (e.g. PS25PolyFR contains 25 wt% PolyFR). PS was used instead of EPS after confirming that both materials exhibit comparable pyrolysis behavior and because it is easier to handle (see Supporting Material). The compositions of PS, PolyFR, and the prepared mixtures are summarized in Table 3. Key physical properties of PS and PolyFR are summarized in Table 4.

To ensure relevance to application conditions, additional mixtures with lower PolyFR contents (0.84, 2.0, and 2.5 wt% PolyFR) were prepared to validate the transferability of the trends observed at elevated loadings. The compositions of these samples are given in Table 5.

The influence of the sample preparation method was also assessed by comparing manually mixed and industrially blended samples. Blended samples were provided by LANXESS AG, and the corresponding results are provided in the Supporting Material. No significant differences in the resulting decomposition behavior were observed.

2.2. Thermogravimetric analysis

Thermogravimetric analysis (TGA) was conducted using a NETZSCH TG 209 F1 Libra equipped with an automatic sampler. 10 mg samples were weighed into Al_2O_3 crucibles without lids. Measurements were performed under a constant nitrogen flow of 60 mL min^{-1}, heating from 40 to 900 °C at a constant heating rate of either 10 or 100 K min^{-1}. Prior to each measurement, samples were purged inside the balance with nitrogen at 40 °C for 30 min. After reaching the final temperature of 900 °C, the atmosphere was switched from nitrogen to synthetic air to oxidize remaining residues and pyrolysis deposits within the crucible and the furnace.

The selected experimental conditions (heating rate, gas flow rate, sample mass, and temperature program) were based on established methods for polymer pyrolysis [38,39] and were validated through preliminary experiments. Particular attention was given to ensuring controlled pyrolytic conditions, reproducible heat and mass transfer, and the avoidance of secondary effects, such as catalytic interactions with the crucible material. Reproducibility was confirmed at 10 and 100

Table 2
Physical properties of the investigated materials.

Sample	Physical form	Color	Density/kg•m^{-3}	Softening/°C
EPS-HBCD	Foam	White	54.6[a]	108[b]
EPS-PolyFR	Foam	White	23.9[a]	108[b]
EPS	Foam	White	26.3[a]	110[b]

[a] Measured bulk density.
[b] Determined using a Netzsch 214 Polyma differential scanning calorimeter (DSC; see Supporting Material).

Table 3
Elemental compositions of PS, PolyFR, and the mixed samples prepared with elevated PolyFR loadings.

Sample	C/wt%	H/wt%	Br/wt%	BFR loading/wt%
PS	92.0[a]	8.1[a]	–	–
PolyFR	N/A[b]	N/A[b]	64[c]	100
PS25PolyFR	N/A[b]	N/A[b]	16[d]	25
PS50PolyFR	N/A[b]	N/A[b]	32[d]	50
PS75PolyFR	N/A[b]	N/A[b]	48[d]	75

[a] Determined on a dry basis using a LECO elemental analyzer (Truspec CHN Micro).
[b] N/A: not applicable. Analysis not possible due to bromine interference, composition not calculable.
[c] Disclosed [13].
[d] Calculated based on mixture composition.

Table 4
Key physical properties of PS and PolyFR.

Sample	Physical form	Color	Density/kg•m^{-3}	Softening/°C
PS	Granules	Colorless	1040[a]	102[a]
PolyFR	Powder	White	582[b]	120[c]

[a] Disclosed [37].
[b] Measured bulk density.
[c] Disclosed [13].

Table 5
Elemental compositions of the mixed samples prepared with application-relevant PolyFR loadings.

Sample	C/wt%	H/wt%	Br/wt%	BFR loading/wt%
PS0084PolyFR	N/A[a]	N/A[a]	0.5[b]	0.84
PS020PolyFR	N/A[a]	N/A[a]	1.3[b]	2.0
PS025PolyFR	N/A[a]	N/A[a]	1.6[b]	2.5

[a] N/A: not applicable. Analysis not possible due to bromine interference, composition not calculable.
[b] Calculated based on mixture composition.

K•min^{-1} by replicate measurements. No significant influence of sample preparation or experimental parameters on the resulting mass loss profiles was observed.

Unless otherwise stated, experiments were conducted in quadruplicate and the resulting mass loss curves were averaged. Because both HBCD and PolyFR act primarily in the gas phase, mass loss curves obtained from TGA were converted to volatile formation curves as per Netsch et al. [38]. The derivative mass loss curves were converted to volatile formation rate curves in the same manner.

Interactions between PolyFR and PS were evaluated by comparing experimental and theoretical volatile formation and volatile formation rate curves for the mixtures containing 25, 50, and 75 wt% PolyFR. Experimental mass loss and derivative mass loss curves were obtained via TGA. Theoretical curves were generated in the Netzsch Proteus Thermal Analysis Software [40] by arithmetically superimposing the individual PS and PolyFR curves according to their respective mass fractions in the mixture. This superposition yields a weighted average of the PS and PolyFR contributions at each temperature. Theoretical mass loss $Mass\ loss_{theo.}(T)$ was calculated using Eq. 1, where x_{PS} and x_{PolyFR} denote the mass fractions of PS and PolyFR in the mixture, and $PS(T)$ and $PolyFR(T)$ represent the temperature-dependent mass loss profiles of the individual components. The derivative of $Mass\ loss_{theo.}(T)$ was defined as the theoretical derivative mass loss. The resulting theoretical mass loss and derivative mass loss curves were subsequently converted to volatile formation and volatile formation rate curves for comparison with the experimental data.

$$Mass\ loss_{theo.}(T) = x_{PS} \bullet PS(T) + x_{\mathrm{PolyFR}} \bullet PolyFR(T) \quad (1)$$

2.3. Fourier-transform infrared spectroscopy

A Bruker Vertex 80v Fourier-transform infrared (FTIR) spectrometer coupled to the NETZSCH TG 209 F1 Libra Thermogravimeter (TG) was used to monitor HBr evolution during pyrolysis. The coupled system (TG-FTIR) proved effective for investigating evolving gases in complex mixtures [41,42]. The FTIR was coupled to the TG following the setup described by Zeller et al. using a heated polytetrafluoroethylene (PTFE) transfer line [43]. Both, the TG outlet interface and the transfer line were kept at 230 °C to prevent product condensation, while the infrared cell temperature was set to 200 °C.

A background spectrum was recorded after a 30-min nitrogen purge of the system and before starting each TG measurement. Volatile species were analyzed across a wavenumber range of 600–4000 cm^{-1} at a spectral resolution of 2 cm^{-1}. This spectral resolution was selected based on preliminary tests, which showed that higher resolutions lead to the splitting of the HBr peak. For measurements performed at 5, 10, and 100 K•min^{-1}, 64 scans per spectrum were collected, corresponding to measurement intervals of 13 s. This number of scans was selected to optimize the signal-to-noise (S/N) ratio while maintaining sufficiently short measurement intervals to accurately resolve the HBr evolution profiles at the respective heating rates. Unless otherwise stated, HBr evolution profiles from quadruplicate TG-FTIR measurements were evaluated individually and then averaged.

2.3.1. HBr calibration

HBr was calibrated by assuming a linear relation between infrared absorbance and concentration in accordance with the Beer-Lambert law. The Beer-Lambert relationship, given in Eq. 2, is applied in its integral form over a characteristic wavenumber interval (ν_1-ν_2). Here, I is the integrated absorbance, A is the measured absorbance, $\in$ is the extinction coefficient of the target gas, l is the optical path length, and C is the concentration [7].

$$I = \int_{\nu_1}^{\nu_2} A(\nu)\, d\nu = \int_{\nu_1}^{\nu_2} \in(\nu) lC\, d\nu \quad (2)$$

The HBr concentration was determined using the integral of the absorbance band 2621 cm^{-1}, evaluated over the range 2620–2622 cm^{-1}. This spectral region was selected because it remains free of overlapping absorption bands from other species throughout the measurement.

The FTIR spectrometer was calibrated with certified HBr/N_2 reference gas mixtures which were introduced into the FTIR via the TG outlet interface. Calibration parameters, including gas flow, temperature and optical path length of the IR cell, and the optical settings of the FITR spectrometer, were kept identical to those used during the experiments.

The standard deviation of all calibration points was below $1.9{\cdot}10^{-4}$. The highest relative standard deviation (RSD) was observed at 3.2% for the reference gas concentration of 1027 mg m^{-3}. This confirms a high level of precision across the calibration range. A best-fit linear regression was applied to create the calibration curve. The resulting coefficient of determination (R^2) is 0.9981. Both the calibration points and resulting calibration curve are shown in Fig. 3.

To calculate the total mass of detected HBr m_{HBr}, the integral is first converted into time-resolved concentration profiles and then integrated for a temperature range from 40 to 600 °C while considering the purge gas flow. The resulting m_{HBr} is converted into a total mass of bromine released as HBr $m_{Br\ in\ HBr}$ using Eq. 3. Here, M_{HBr} and M_{Br} represent the molecular masses of HBr and Br, respectively. Bromine released as HBr relative to the bromine content introduced by the sample composition $m_{Br\ relative\ to\ input}$ is calculated using Eq. 4, where $m_{Br\ in\ sample}$ represents the bromine content in the sample.

$$m_{Br\ in\ HBr} = \frac{m_{HBr}}{M_{HBr}} \bullet M_{Br} \quad (3)$$

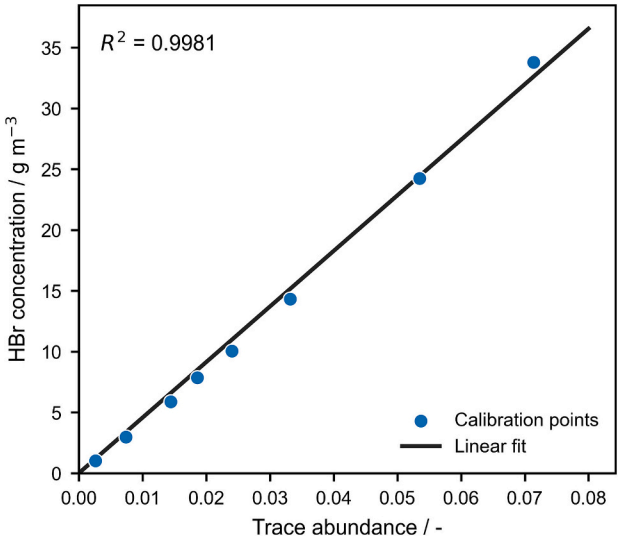

Fig. 3. HBr calibration points and curve.

$$m_{Br\ relative\ to\ input} = \frac{m_{Br\ in\ HBr}}{m_{Br\ in\ sample}} \bullet 100 \quad (4)$$

To ensure that measurements remained within the applicable calibration range, TG-FTIR analyses were performed using sample masses of either 5 or 10 mg, depending on the bromine content and heating rate. At 10 K•min^{-1}, a sample mass of 5 mg was chosen for pure PolyFR and PS75PolyFR as both exhibited the highest HBr yields, while PS25PolyFR and PS50PolyFR were analyzed using a total mass of 10 mg. At 100 K•min^{-1}, PS50PolyFR was analyzed using a total sample mass of 5 mg to account for the more concentrated HBr release occurring over a shorter time at this heating rate.

2.4. Pyrolysis-gas chromatography–mass spectrometry

Pyrolysis-gas chromatography–mass spectrometry (Py-GC–MS) analyses were performed using a CDS Pyroprobe 6200 micropyrolyzer coupled to a 7890B Agilent gas chromatograph and a 5977B Agilent single-quadrupole mass selective detector. The micropyrolyzer was connected to the GC using a heated transfer line maintained at 350 °C. The GC inlet and the GC–MS transfer line were also kept at 350 °C to ensure consistent transfer conditions. The GC was equipped with a 31 m × 250 µm × 0.25 µm Rtx-200MS column from Restek. The split injector was operated at 300 °C and 70 kPa, with a split ratio at 100:1. The MS detection was conducted in positive ion mode in the scan range of mass-to-charge (m/z) 10–600 at a scan frequency of 4.8 Hz.

Approximately 50 µg of sample was used for each measurement. The samples were weighed into quartz glass tubes and secured with chemically inert quartz wool. The tubes were introduced into the pyrolyzer using an automated sampler. After insertion, the reaction chamber was sealed and purged with helium. Pyrolysis was initiated by heating the sample from room temperature to the target temperature at a heating rate of 500 °C s^{-1}, followed by a 1 min isothermal hold. During pyrolysis, the reaction chamber was continuously flushed with helium, transferring volatiles products into the GC. Upon the completion of the 1 min, the sample tube was rapidly cooled back to room temperature, while helium flushing continued for an additional 10 s to ensure complete transfer of analytes. The helium flow rate in the system was regulated by the GC and set to 135 mL min^{-1}.

Two pyrolysis programs were used for the analysis: (i) single-step pyrolysis and (ii) temperature-staged pyrolysis.

In the single-step program, the sample heated to 450 °C for held for 1 min, as described above. During this time, volatile products were continuously transferred to the GC–MS. After completion of the run, the sample tube was removed from the reaction chamber, which was then purged with helium for 10 s. Subsequently, the chamber was isolated from the GC, vented to the atmosphere, and heated to 1000 °C to remove residual deposits.

In the temperature-staged program, pyrolysis was conducted in two sequential steps to enable the separation of low- and high-temperature products. In the first stage, the sample was heated to 350 °C and held for 1 min, while the evolved vapors were transferred to the GC–MS for analysis. After the 1 min, the reaction chamber was flushed with helium and cooled to room temperature. The chamber was then sealed from the GC transfer line, leaving the partially pyrolyzed sample inside.

Following completion of the GC–MS analysis of the first stage, the reaction chamber was reconnected to the GC transfer line. The remaining sample was then heated to 450 °C and held for 1 min, and the resulting vapors were transferred to the GC–MS as a second, separate analysis. After the second stage, the sample tube was removed from the reaction chamber, which was then purged with helium, isolated, vented, and heated to 1000 °C to remove any remaining residues.

For both single-step and staged-pyrolysis analyses, blank runs were performed after each measurement to assess baseline stability and potential carryover of analytes. No significant carryover or baseline drift was observed.

All measurements were performed in triplicate. The resulting chromatograms were normalized to Total Ion Count (TIC) per µg and evaluated individually before averaging. Compound identification was performed using the NIST MS Search v.2.3 database and processed with the open-source software OpenChrom. The influence of HBCD and PolyFR on EPS pyrolysis was evaluated by comparing the relative peak areas of the styrene monomer (C_8H_8), dimer ($C_{16}H_{16}$), and trimer ($C_{24}H_{24}$). The dimer was identified by the peak corresponding to 1,4-diphenyl-2-butene and the trimer by 1,3,5-triphenylcyclohexane. The product distribution of PolyFR was evaluated in the same manner, in addition to considering the relative peak areas of HBr and other brominated species.

Peak detection was performed with a minimum S/N ratio of 3. Peaks not automatically detected with this detection threshold were manually inspected and integrated, if they were clearly resolved above the baseline and consistently observed across replicate measurements.

As no external calibration was performed, the analysis is semi-quantitative. Peak height and relative peak area have been reported to provide an indication of the relative contributions of species to the overall product distribution [44,45]. Accordingly, conclusions regarding the influence of BFRs are based on changes that exceed the variability observed between replicate measurements.

Reproducibility was assessed using multiple metrics. First, the similarity between chromatograms was evaluated by calculating the mean pairwise Pearson correlation coefficient ($\bar{r}$) of mass-normalized TIC profiles for all replicate pairs. The resulting $\bar{r}$ values are above 0.94, indicating high similarity between chromatograms. $\bar{r}$ was calculated using Eq. 5 and Eq. 6, where x and y represent individual runs (e.g. r_{12} corresponds to runs 1 and 2), x_i and y_i denote the TIC intensities at each retention time, $\bar{x}$ and $\bar{y}$ are the corresponding mean values, and n is the number of data points.

$$r_{xy} = \frac{\sum_{i=1}^{n}(x_i - \bar{x})(y_i - \bar{y})}{\sqrt{\sum_{i=1}^{n}(x_i - \bar{x})^2}\sqrt{\sum_{i=1}^{n}(y_i - \bar{y})^2}} \quad (5)$$

$$\bar{r} = \frac{r_{12} + r_{13} + r_{23}}{3} \quad (6)$$

Second, the RSD of the integrated areas of the three dominant peaks (accounting for approximately 96–97% of the total integrated peak areas) was evaluated. A maximum RSD of 3% was observed, indicating high reproducibility. Third, retention time stability of the main peak was assessed, with a maximum standard deviation (SD) of 0.037 min. Individual chromatograms and peak area analyses are provided in the Supporting Material.

PolyFR was analyzed in its powder form. EPS, EPS-HBCD, and EPS-PolyFR samples were prepared by cutting material from the EPS panels using a scalpel. The spatial distribution of PolyFR within the EPS matrix was evaluated by Scanning Electron Microscopy with Energy-Dispersive X-ray Spectroscopy (SEM-EDX), with the corresponding images provided in the Supporting Material. The SEM-EDX mapping of bromine and carbon indicates that PolyFR is distributed throughout the EPS matrix, rather than being present as isolated agglomerates. Together with the high reproducibility of the chromatograms and product distributions, this supports that the investigated samples are representative under the applied experimental conditions.

3. Results and discussion

3.1. Pyrolysis of commercial flame-retarded and non-flame-retarded EPS

3.1.1. Decomposition behavior via TGA

The volatile formation and volatile formation rate curves obtained for commercial EPS, waste EPS-HBCD, and commercial EPS-PolyFR are shown in Fig. 4a and Fig. 4b. At 10 K•min^{-1}, all three samples decompose predominately from 350 to 450 °C, with a 50 wt% volatilization occurring at approximately 415 °C.

EPS exhibits an onset of decomposition, defined at 5 wt% volatilization, at 378 °C. Decomposition progresses to leave no residue at 445 °C. This behavior is characteristic of styrenic polymers [21]. In contrast, EPS-HBCD shows an onset temperature 17 °C lower than that of EPS and leaves 1.4 wt% residue at 467 °C, which remains relatively constant beyond this temperature. This behavior has been attributed to the homolytic cleavage of the first C—Br bond in HBCD [7,32]. EPS-PolyFR also exhibits a reduced onset temperature, 21 °C below that of EPS, and leaves less than 0.5 wt% residue at 469 °C.

Despite the difference in chemical structure, both HBCD and PolyFR induce comparable reductions in the onset temperature. This behavior can be attributed to intrinsic properties of BFRs. One the one hand, C—Br bonds in BFRs have relatively low bond dissociation energies in comparison to C—C or C—H bonds [32,46], thus promoting bond cleavage and volatilization at lower temperatures. On the other hand, cleavage of C—Br bonds in HBCD and PolyFR promotes a catalytic effect through mechanisms such as autocatalytic chain scission, whereby radical species accelerate PS decomposition [33,47]. As a result, an earlier decomposition is observed for the HBCD- and PolyFR-containing EPS curves compared to non-flame-retarded EPS.

At 407 °C, the volatile formation curves of the three samples intersect in Fig. 4a. Above this temperature, the relative slopes of the curves reverse compared with lower temperatures. The EPS curve becomes steeper than the EPS-HBCD and EPS-PolyFR curves, indicating higher volatilization at equivalent temperatures. The delayed volatile formation observed for EPS-HBCD and EPS-PolyFR is reflected in Fig. 4b by a shift of the volatile formation rate peaks to slightly higher temperatures and a reduction in the maximum volatilization rate. These observations indicate a slight stabilization effect, potentially associated with the formation of relatively stable intermediates that delay PS volatilization at elevated temperatures.

3.1.2. Product analysis via Py-GC–MS

To evaluate the effect of HBCD and PolyFR on EPS pyrolysis products, the product spectra and distribution of the main products are compared. The results are shown in Fig. 5.

The product spectra in Fig. 5a show that EPS, EPS-HBCD, and EPS-PolyFR predominantly decompose into styrene monomer (C_8H_8), dimer ($C_{16}H_{16}$), and trimer ($C_{24}H_{24}$).

The relative product distribution shown in Fig. 5b was obtained by comparing the absolute peak areas of the styrene monomer, dimer, and trimer, normalized to 1 µg. These three products account for more than 95% of the respective total peak area across the chromatograms of the three samples. As mentioned in Section 2.4, the reported peak areas serve only as a semi-quantitative indication of the relative contributions of these species to the overall product distribution [44,45]. In Fig. 5b, styrene monomer constitutes 75–78% of the detected peak areas, while the dimer and trimer contribute 7–8% and 12–13%, respectively. These results indicate that, under the investigated conditions and at the applied BFR loadings, neither HBCD nor PolyFR significantly influences the distribution of the dominant monomer, dimer, and trimer species.

In addition to the monomer, dimer, and trimer, EPS spectra contain minor peaks corresponding to toluene, α-methylstyrene, and bibenzyl, as well as ethylbenzene, cumene, and derivatives of the dimer and trimer. This is in agreement with the literature [23,27,48]. Similarly, EPS-HBCD produces minor peaks corresponding to toluene and α-methylstyrene, along with dimer and trimer derivatives. EPS-PolyFR shows a comparable product profile, with minor peaks attributed to toluene, α-methylstyrene, bibenzyl, and 1,3-diphenylpropane, as well as dimer and trimer derivatives. These observations further support that

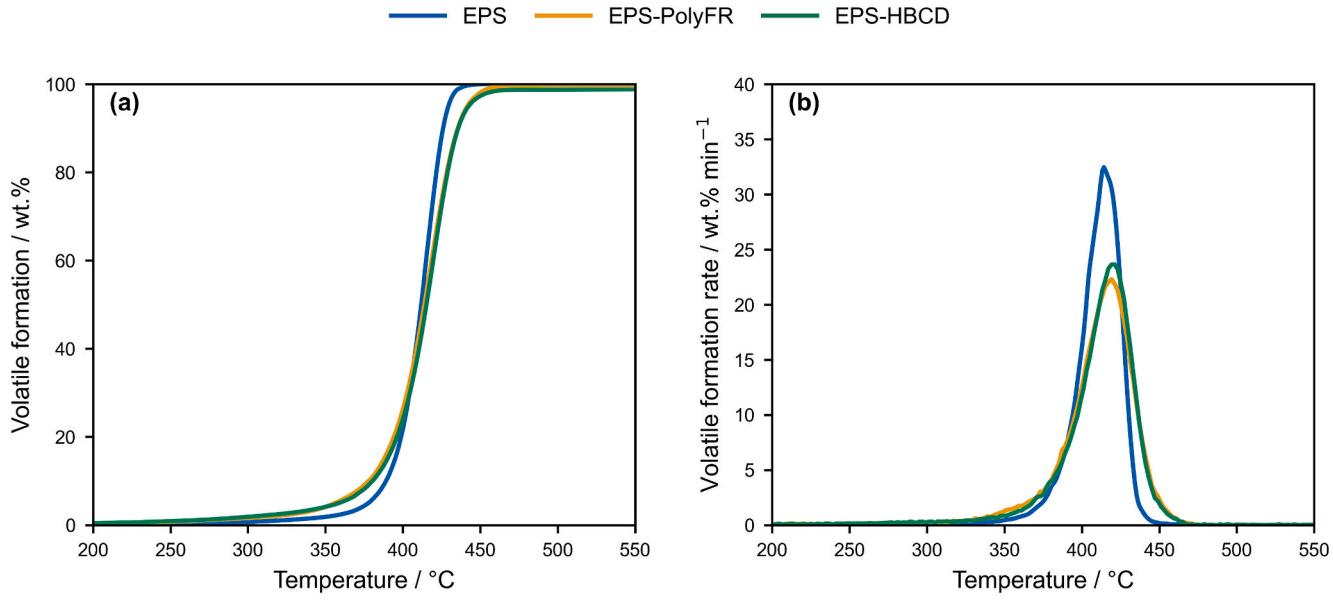

Fig. 4. (a) Volatile formation and (b) volatile formation rate curves obtained using 10 mg of EPS, EPS-HBCD, and EPS-PolyFR, measured at 10 K•min^{-1}.

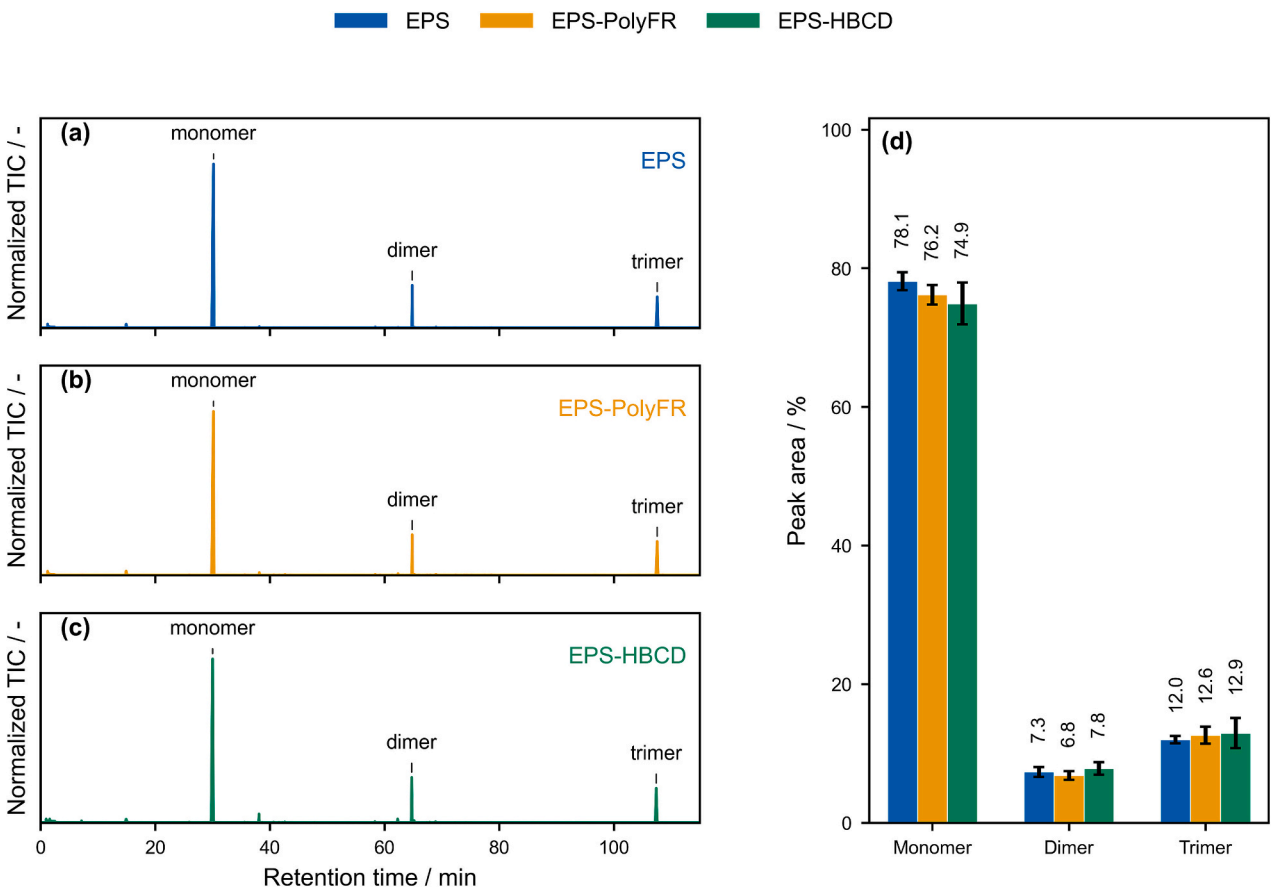

Fig. 5. (a) EPS, EPS-PolyFR, EPS-HBCD pyrolysis chromatograms at 450 °C and (b) the corresponding relative peak area distribution of styrene, dimer, and trimer.

the presence of HBCD or PolyFR, under the investigated conditions, does not significantly alter the overall product distribution of EPS pyrolysis.

The analysis provides no evidence for the presence of HBr in the spectra of EPS-HBCD and EPS-PolyFR. Given the low bromine contents in both samples (0.2 and 0.3 wt%), HBr remains below detection limits (S/N ratio of 3), even when targeting the characteristic HBr *m/z*-quadruplet 79, 80, 81, 82 [49]. As for brominated hydrocarbons, only (1-bromo-1-methylethyl)benzene is identified in EPS-PolyFR spectra, though at very low intensities and negligible overall contribution.

Studies investigating PS with higher HBCD contents (approximately 1.8 wt% bromine) reported a distinct HBr peak at 400 °C using Py-GC–MS [32]. HBr formation from the commercial samples examined in the current study therefore cannot be ruled out. Samples prepared with higher BFR loading are examined and discussed in Section 3.3.

Overall, the product spectra indicate that, under the investigated conditions and at bromine levels representative of real EPS waste, neither HBCD nor PolyFR leads to pronounced changes in the pyrolysis product distribution. The dominance of styrene-based product spectra and the absence of detectable brominated species suggest that pyrolysis of flame-retarded EPS can, in principle, yield pyrolysis oils comparable to those obtained from non-flame-retarded EPS. From a recycling perspective, these observations are encouraging, as they imply that product quality is not compromised for the investigated samples.

Nevertheless, it is important to consider that the absence of observable effects may be related to the low bromine contents, which approach the detection limits of GC–MS analysis. Alternatively, it may reflect limited interactions between the flame retardants and the PS matrix under the applied conditions. Distinguishing between these possibilities is critical for evaluating the general applicability of pyrolysis-based recycling and is therefore examined in the subsequent sections of this work, beginning with an investigation of the pyrolysis behavior of PolyFR in Section 3.2, followed by an evaluation of PolyFR-PS interactions at higher BFR loadings in Section 3.3.

3.2. *Pyrolysis of PolyFR*

3.2.1. *Decomposition behavior via TGA and TG-FTIR*

To characterize the decomposition behavior of PolyFR under pyrolytic conditions, the volatile formation and volatile formation rate curves were obtained, and HBr evolution was evaluated. Both curves, in addition to the HBr evolution profile, are shown in Fig. 6.

Pure PolyFR decomposes in two distinct temperature ranges distinguished by the inflection point in the volatile formation curve marked by the dashed line at 341 °C in Fig. 6. The onset of decomposition is observed at 253 °C. The first decomposition step, defined by volatilization below 341 °C, accounts for approximately 67 wt% volatilization in Fig. 6a and results in a narrow and sharp peak in the volatile formation rate curve in Fig. 6b, indicating rapid volatilization. The peak reaches a maximum of 38.7 wt% min^{-1} at 260 °C. The second decomposition step contributes an additional 24.4 wt% volatilization and results in 7.3 wt% residues at 526 °C. The residue decreases to 7 wt% at 700 °C and remains stable thereafter. The corresponding peak in the volatile formation rate curve is broader than the first and reaches a maximum of 3.5 wt% min^{-1} at 450 °C, reflecting slower volatile release compared to the first step. This stabilization effect is likely due to the formation of relatively stable tertiary radicals that delay backbone scission, or to double bonds that form on isolated side chains upon bromine elimination from 1,2-isomeric units [12].

TG-FTIR analysis shows that HBr forms in the first decomposition step from 235 to 334 °C, reaching a maximum concentration at 265 °C. FTIR bands corresponding to other volatile components appear from 387 °C onward in the wavenumber range 2825–3141 cm^{-1}, a band

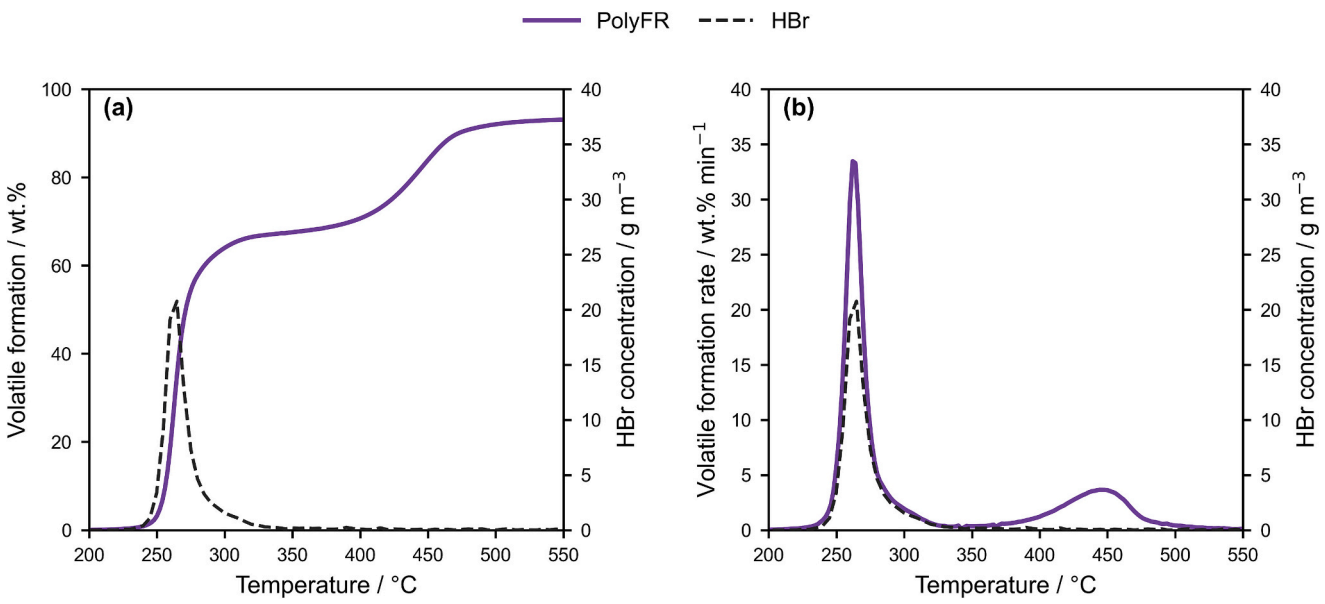

Fig. 6. HBr evolution profile overlaid on the (a) volatile formation and (b) volatile formation rate curves, obtained using 5 mg PolyFR at 10 K•min^{-1}.

which is characteristic of hydrocarbons [39]. This suggests that peak volatilization in the first and second decomposition steps proceeds independently.

The detected HBr accounts for 89 wt% of the total bromine content in PolyFR. This value is based on quadruplicate measurement with a SD of 2.2 wt%. The method was evaluated in duplicate at a heating rate of 5 K•min^{-1}. The resulting bromine recovered as HBr amounts to 90 wt% with a SD of 0.3 wt%. This confirms reproducibility of results and the suitability of the FTIR method.

While Br_2 formation cannot be assessed using IR techniques, Barontini et al. excluded its formation during HBCD pyrolysis by iodometric titration of pyrolysis gases [7]. The same conclusion was reported by Larsen and Ecker [34]. Given the similar bromine radical activity and HBr formation behavior in HBCD and PolyFR [7,12,32], Br_2 formation in PolyFR pyrolysis is assumed to be negligible. The remaining 11 wt% of bromine not detected as HBr is therefore assumed to be either released in the volatile fraction in forms other than HBr or retained in the solid residue.

Residue analysis was not performed due to the limited amount of solid material generated. Consequently, the presence of brominated hydrocarbons in the solid fraction cannot be confirmed and requires further investigation.

As for the volatile fraction, TG-FTIR does not resolve the complete molecular composition of complex mixtures due to compound-specific absorption coefficients and detection limits, which may hinder the detection of low-concentration species. In addition, overlapping absorption bands from organic pyrolysis products can obscure the presence of further brominated compounds. The analytical approach was therefore not intended to identify all brominated species. In contrast, HBr exhibits distinct spectral features even in complex mixtures. Hence, TG-FTIR parameters were specifically optimized for its reliable detection and quantification.

3.2.2. Product analysis via Py-GC–MS

To complement the TG-FITR analysis, Py-GC–MS was used to characterize the molecular composition of volatile products formed during PolyFR pyrolysis, with particular focus on brominated species. The results are shown in Fig. 7.

HBr is observed at the beginning of the chromatogram in Fig. 7a. The broad, asymmetric, tailing peak is consistent with reported HBr behavior [32]. This shape is typical of small, highly polar, and reactive gases in GC systems, arising from interactions with active sites in the injection system and along the GC column which retard elution [50]. HBr contributes approximately 16% of the total peak area, as shown in Fig. 7b. Minor peaks of mono-brominated C9 and C10 aromatic compounds such as (1-bromo-1-methylethyl)benzene, 1-bromomethyl-4-isopropylbenzene, and 1-bromo-4-phenylbutane are identified. These account for less than 1% of the total detected peak area. The suggests that bromine is released predominantly as HBr during PolyFR pyrolysis, consistent with TG-FTIR observations.

PolyFR also decomposes into products characteristic of styrene decomposition. The styrene-dimer-trimer triplet observed in Fig. 7 stems from the PS blocks in the triblock structure of PolyFR. Styrene shows the highest peak intensity and the largest relative peak area. Toluene (C_7H_8), ethylbenzene (C_8H_{10}), and α-methylstyrene (α-C_9H_{10}) are also present, though exhibit higher peak intensities in PolyFR than in EPS. This is likely due to a mechanism similar to the so-called 'enhanced decomposition', which PolyFR induces when blended with PS. This mechanism refers to the homolytic cleavage of PolyFR to generate a radical initiator that abstracts hydrogen from the PS backbone, forming a PS radical that subsequently undergoes β-scission [11]. The formation of α-methylstyrene is favored by tertiary radicals at the α-carbon adjacent to the aromatic ring, which is prone to β-scission [48]. Ethylbenzene is formed through alkyl transfer and recombination reactions, and its formation persists under catalytic conditions [51]. The presence of toluene, ethylbenzene, and α-methylstyrene suggests that, in the absence of an external PS matrix, PS blocks within the triblock structure of PolyFR act as hydrogen donors, thereby promoting radical-driven reactions. These interactions promote chain scission and alkyl transfer, leading to increased formation of low-molecular-weight aromatic compounds relative to EPS.

3.3. Interactions between PolyFR and PS

3.3.1. Superposition

Interactions between PolyFR and PS were evaluated by comparing experimental and theoretical volatile formation and volatile formation rate curves for mixtures containing 25, 50, and 75 wt% PolyFR. These elevated PolyFR contents were selected to amplify potential interactions between PolyFR and PS and to overcome limitations associated with low bromine levels at application-relevant loadings. The theoretical curves were obtained by superimposing the individual contributions of PS and

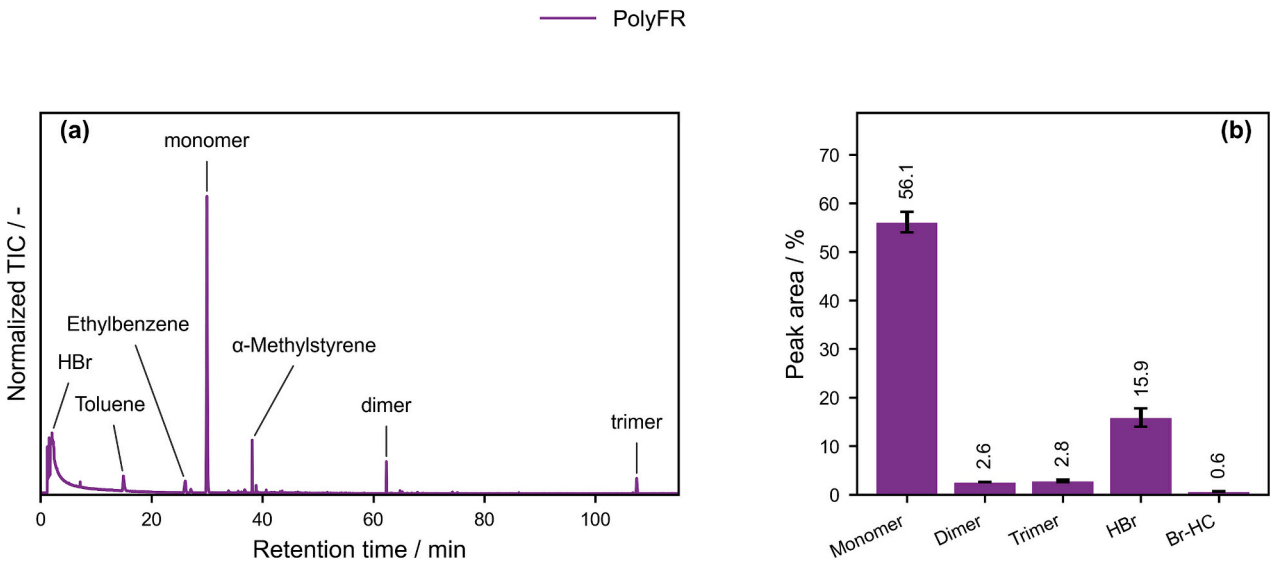

Fig. 7. (a) PolyFR pyrolysis chromatogram at 450 °C, and (b) the corresponding relative peak area distribution of styrene, dimer, trimer, HBr, and brominated hydrocarbons (Br-HC).

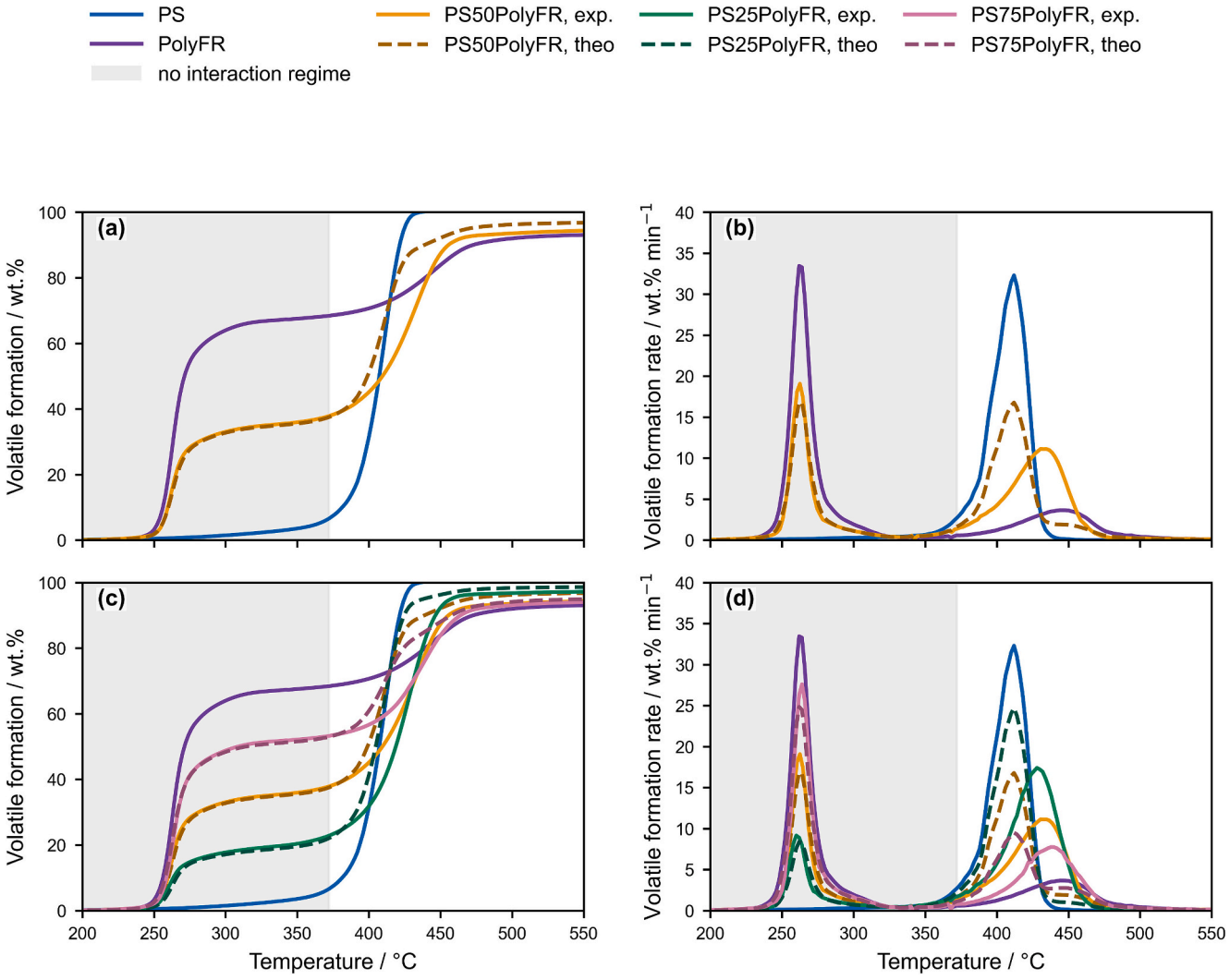

Fig. 8. Experimental (exp.) and theoretical (theo.) volatile formation and volatile formation rate curves of PS, PolyFR, and their mixtures containing 25, 50, 75 wt% PolyFR at 10 K•min^{-1}. Experimental curves were obtained using 10 mg of PS25PolyFR and PS50PolyFR and 5 mg of PS75PolyFR.

PolyFR, as described in Section 2.2. The resulting curves, together with those of pure PS and PolyFR, are shown in Fig. 8.

Fig. 8a and Fig. 8b present the experimental and theoretical volatile formation and volatile formation rate curves for the 50 wt% PolyFR mixture, together with the experimental curves of pure PS and PolyFR. The curves overlap up to approximately 372 °C, indicating that no measurable interaction between PS and PolyFR occurs within this temperature range. This temperature is therefore taken as the upper limit of the non-interacting regime. At higher temperatures, deviations between experimental and theoretical behavior become apparent, marking the onset of interaction effects. The same trend is observed for the mixtures containing 25 and 75 wt% PolyFR, as shown in Fig. 8c and Fig. 8d.

The lack of interaction between PS and PolyFR during the first PolyFR decomposition step is further supported by comparing the experimental and theoretical volatile yields of the investigated mixtures. Table 6 shows that across all mixtures, the theoretical curves predict volatile yields in close agreement with those obtained experimentally at 372 °C.

A kinetically relevant interaction between PS and the remaining PolyFR chain becomes apparent beyond 372 °C, as the experimental and theoretical curves diverge. This divergence indicates that decomposition kinetics deviate from independent behavior, pointing to interaction between PS-derived radicals and PolyFR decomposition intermediates. The volatile formation rate peaks associated with the second decomposition step differ in both magnitude and position, as shown in Fig. 8b and Fig. 8d. Experimentally, increasing PolyFR loading leads to a decrease in the maximum volatilization rate and a shift of this maximum to higher temperatures. The calculated curves predict a decrease in the maximum volatilization rate with increasing PolyFR loading; however, the temperature of maximum volatilization remains constant at 412 °C across all compositions. For all mixtures, the experimental maximum volatilization rates are lower than those obtained from the calculated curves. Furthermore, both the experimental and theoretical volatile formation curves show increasing residual mass at 550 °C with higher flame-retardant content. The theoretical values, however, consistently underestimate the experimentally observed residue. These findings, as summarized in Table 7, indicate that the thermal decomposition of PS-PolyFR mixtures involves interactions that are not captured by the calculated superposition curves.

The delayed volatilization in the second decomposition step of the prepared mixtures and the corresponding shift of the volatile formation rate peak to higher temperature indicate a stabilization effect. This effect becomes more evident with increasing PolyFR loadings, as the volatile formation curves become less steep and the corresponding volatile formation rate peaks broaden and decrease in height. The reduced peak height further suggests slower decomposition kinetics or an increased activation barrier for this step.

The observed stabilization effect can be rationalized by considering the interaction between PS-derived radicals and PolyFR decomposition intermediates. During PS pyrolysis, intermolecular hydrogen transfer and β-scission sustain depolymerization [11,26] as unsaturated chain ends formed between 350 and 500 °C readily undergo scission to generate additional radicals [52]. This process depends on the availability and mobility of reactive radical species.

In contrast, the first decomposition step of PolyFR involves dehydrobromination of the 1,4-polybutadiene segment, leading to the formation of conjugated polyenes [12,53]. These unsaturated intermediates can act as radical acceptors or participate in addition reactions with PS-derived radicals. Such interactions reduce the availability of free radicals required for chain transfer and propagation, thereby suppressing the depolymerization rate. Furthermore, the formation of conjugated intermediates promotes crosslinking reactions, as suggested by the exothermic DSC signal reported by Wang et al. [11] and confirmed by our own DSC analysis (see Supporting Material). The resulting crosslinked structures restrict the mobility of reactive species, further contributing to an increased effective activation barrier.

Table 6
Comparison between the experimental and theoretical volatile yields at 372 °C.

Sample	Experimental volatile yield/wt%	Theoretical volatile yield/wt%
PS25PolyFR	22.8	22.0
PS50PolyFR	37.9	37.5
PS75PolyFR	53.2	52.9

Table 7
Comparison between the experimental (exp.) and theoretical (theo.) volatile formation rate peaks corresponding to the second decomposition step.

Sample	Maximum volatilization rate/% min^{-1}	Temperature of maximum volatilization rate/°C	Residue at 550 °C/wt%
PS25PolyFR exp.	17.4	428	2.8
PS25PolyFR theo.	24.7	412	1.4
PS50PolyFR exp.	11.1	435	5.8
PS50PolyFR theo.	16.8	412	4.0
PS75PolyFR exp.	7.7	438	6.0
PS75PolyFR theo.	9.5	412	5.1

The increased experimental residue relative to the theoretical superposition can likewise be attributed to interactions between reactive PS-derived species and PolyFR-derived polyenes, leading to the formation of additional crosslinked or condensed structures.

Similar behavior has been reported for PS-PVC blends, which also undergo multi-step decomposition characterized by an initial dehydrohalogenation step [38,52]. Dodson and McNeill argued that disrupting the intermolecular transfer reactions during PS pyrolysis is an effective stabilization pathway [52]. Polyenes formed from PVC were shown to interfere with these reactions, thereby delaying PS decomposition. This effect became more pronounced with increasing PVC loadings [38,52]. This trend is consistent with the present observations, where increasing PolyFR loading leads to stronger stabilization effects.

In the case of HBCD, interactions with the PS matrix cannot be assessed experimentally at elevated HBCD loadings, due to regulatory restrictions and are therefore inferred from literature. At 10 wt% loading, HBCD-containing PS exhibits a multi-step decomposition behavior. HBCD decomposes between 200 and 300 °C and its decomposition products interact with the PS matrix to form a thermally resistant fraction that decomposes around 400 °C [54]. This behavior indicates that HBCD can participate in condensed-phase interactions that influence the thermal decomposition pathway of PS [32,54]. Consequently, the comparison between HBCD and PolyFR is limited to application-relevant loadings (see Section 3.1) and qualitative mechanistic considerations.

3.3.2. *Effect of composition on HBr yield*

The absence of apparent interactions between PolyFR and PS until 372 °C, as discussed in the previous section, indicates that the first PolyFR decomposition step proceeds independently of mixture composition. This interpretation is supported by the results in Table 8, which show that all mixtures display an inflection in their volatile formation and volatile formation rate curves at 342 °C. This observation suggests that dehydrobromination follows a similar pathway and concludes at the same temperature across all mixtures. The slight increase in the inflection point temperature in the mixtures compared to pure PolyFR is likely attributable to the fact that PolyFR begins to decompose while within the molten PS matrix.

The results in Table 8 show that volatile yield at the inflection point increases with increasing PolyFR loading and correlates linearly with the bromine content in the mixture. This trend indicates that volatilization during the first PolyFR decomposition step is associated with bromine elimination, as higher PolyFR loadings lead to proportionally greater volatilization. The linear correlation further suggests that bromine elimination is largely independent of mixture composition.

Table 8
Summary of experimental observations associated with the first decomposition step of PolyFR in pure form and in mixtures.

Sample	Bromine content/ wt%	Inflection point/°C	Volatile yield at inflection point/wt%	Bromine detected as HBr[a]/ wt%	SD of bromine[b]/ wt%
PS25PolyFR	16.0	342	19.9	92.3	2.5
PS50PolyFR	32.0	342	35.6	87.2	1.2
PS75PolyFR	48.0	342	51.9	89.9	0.9
PolyFR	64.0	341	67.2	89.0	2.2

[a] Quantified using TG-FTIR relative to the total bromine content in the sample based on composition; values represent the mean of quadruplicate measurements.
[b] SD of bromine detected as HBr calculated from quadruplicate measurements.

This interpretation is supported by TG-FTIR analyses, which show that approximately 90 wt% of the bromine initially present in the samples is detected as HBr across all mixtures, regardless of PolyFR loading.

To evaluate the transferability of these observations to application-relevant PolyFR loadings, the effect of composition on HBr evolution was further investigated using mixtures containing 2.5, 2.0, and 0.84 wt % PolyFR. The corresponding volatile formation and volatile formation rate curves are shown in Fig. 9 alongside the pure PS curves.

A slight shoulder is observed in the volatile formation curves between 250 and 274 °C in Fig. 9a, accompanied by a corresponding minor peak in the volatile formation rate curves in Fig. 9b. The corresponding HBr evolution profiles presented in Fig. 10b and Fig. 10c indicate that HBr is released within this temperature range. At the observed S/N ratio, the data support a qualitative assessment of HBr release. Nevertheless, FTIR analysis shows that HBr is released even at low PolyFR loadings comparable to application-relevant concentrations.

Although the PolyFR loadings in PS020PolyFR and PS025PolyFR fall within application-relevant ranges, they contain more bromine than the commercial EPS-PolyFR and waste EPS-HBCD samples discussed in Section 3.1. As a result, the lower bromine contents in those flame-retarded EPS samples lead to the absence of a visible shoulder in the volatile formation curves and a corresponding minor peak in the volatile formation rate curves in Fig. 4. A similar behavior is observed for PS0084PolyFR, whose HBr evolution profile shown in Fig. 10a exhibits no clearly resolved HBr signal above the baseline noise. Nevertheless, the presence of flame retardants in both the flame-retarded EPS samples and the prepared PS-PolyFR mixtures induces a similar overall thermal behavior. In all cases, the presence of flame retardants leads to an earlier decomposition onset compared with non-flame-retarded EPS and PS, as well as a shift of the volatile formation rate peak to slightly higher temperatures and a reduction in the maximum volatilization rate. Together, these observations indicate a modest stabilization effect at elevated temperatures and demonstrate that PS-PolyFR mixtures containing application-relevant PolyFR loadings reproduce the key thermal features observed for flame-retarded EPS.

3.4. *Effect of heating rate and temperature-staging*

To investigate the effect of heating rate on the observed pyrolysis behavior, additional TG-FTIR experiments were performed at a heating rate of 100 K•min^{-1}. While experiments conducted at 10 K•min^{-1} provide valuable mechanistic insight and support in understanding bromine transfer pathways, the higher heating rate better reflects the rapid thermal exposure experienced by polymeric materials in technical pyrolysis reactors. The corresponding time-resolved results are presented in Fig. 11. The transformation to temperature-resolved data is provided in the Supporting Material.

At 100 K•min^{-1}, volatile formation occurs earlier and is confined to a significantly narrower time interval compared to 10 K•min^{-1}, as reflected by the different time scales in Fig. 11. Despite this temporal compression, the volatile formation curve shown in Fig. 11a follows a similar overall behavior to that observed at 10 K•min^{-1} in Fig. 11d. The shorter volatilization duration leads to a higher apparent formation rate, which is evident when comparing the volatile formation rate curves obtained at 100 K•min^{-1} and 10 K•min^{-1} in Fig. 11b and Fig. 11e, respectively.

Consistent with this behavior, the HBr evolution profile appears earlier at the higher heating rate and exhibits a higher maximum intensity. At 100 K•min^{-1} (Fig. 11c), HBr release occurs within approximately 3 min, compared with approximately 15 min at 10 K•min^{-1} (Fig. 11f), resulting in a higher maximum concentration over the shorter evolution period.

Duplicate measurements at 100 K•min^{-1} show that 75 wt% of the bromine initially present in the sample is detected as HBr, with a variation of ±0.1 wt% between the two measurements, compared with 87 ± 1.2 wt% at 10 K•min^{-1}. As explained in Section 3.3, measurements at

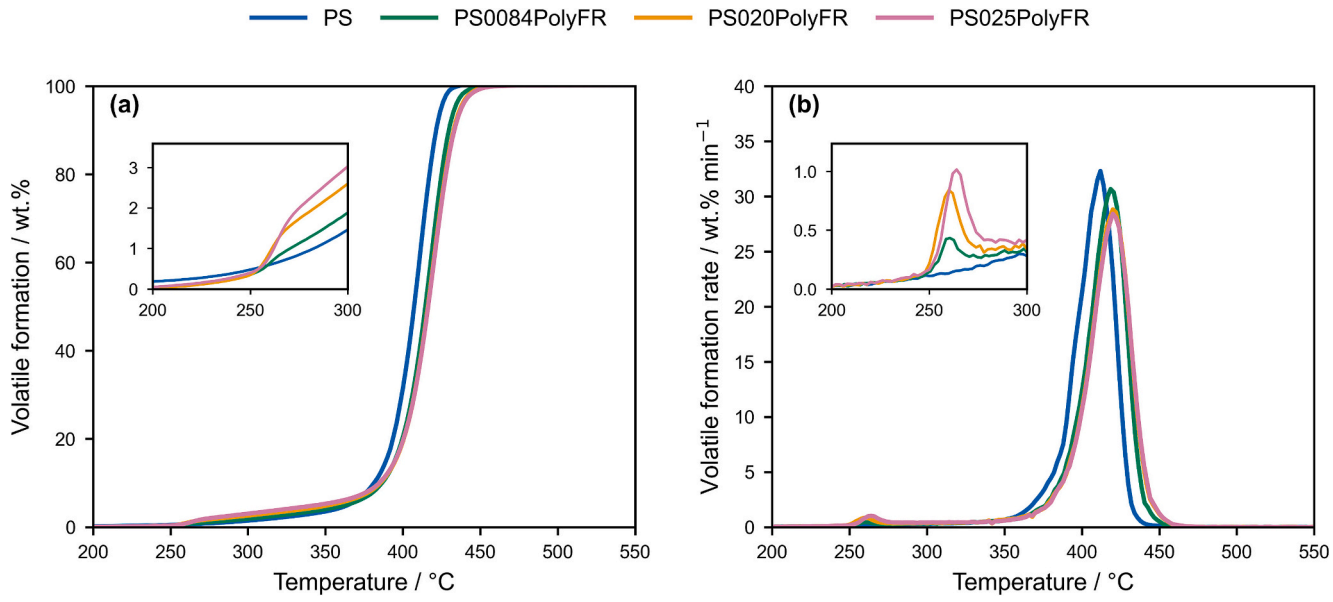

Fig. 9. (a) Volatile formation and (b) volatile formation rate curves of PS and PS-PolyFR mixtures containing 0.84, 2.0, and 2.5 wt% PolyFR, obtained using 10 mg samples at 10 K•min^{-1}.

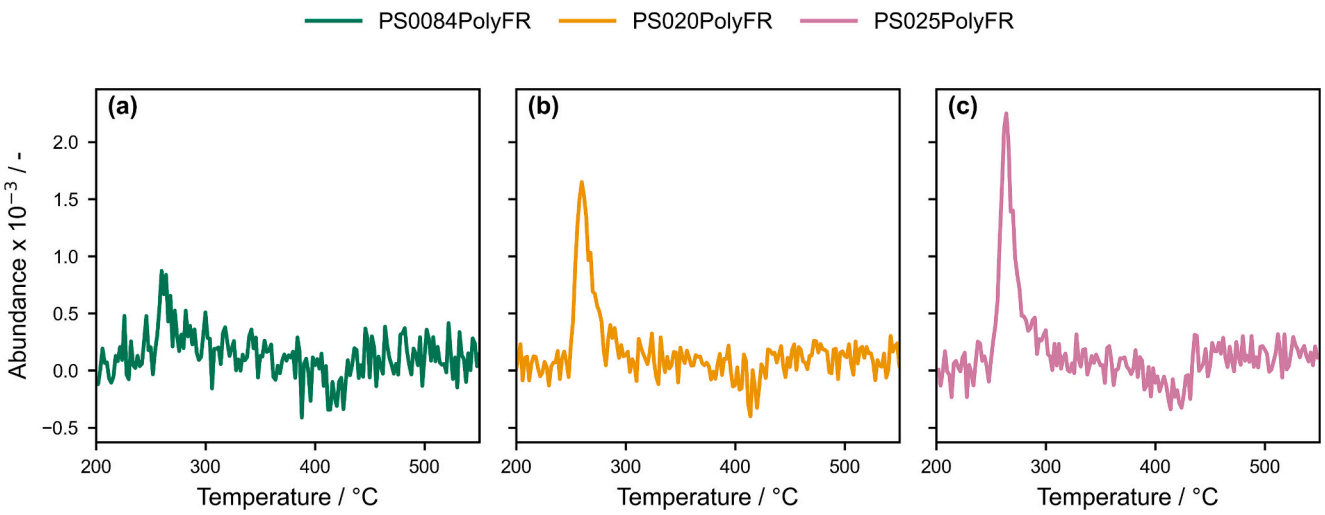

Fig. 10. HBr evolution profiles obtained using 10 mg PS-PolyFR mixtures containing (a) 0.84, (b) 2.0 and (c) 2.5 wt% PolyFR at 10 K•min^{-1}.

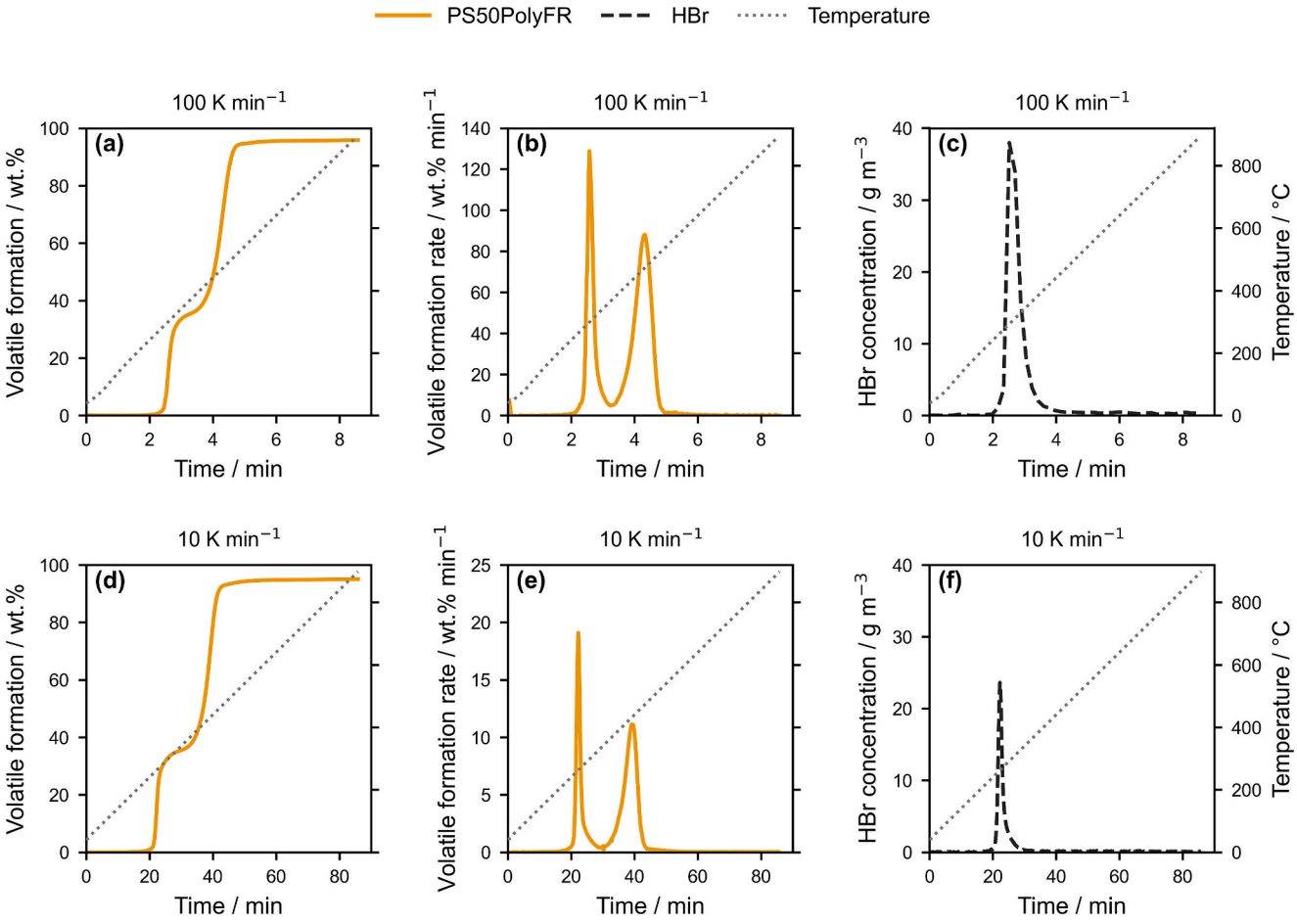

Fig. 11. Time-resolved (a) volatile formation, (b) volatile formation rate, and (c) HBr evolution profiles obtained at 100 K•min^{-1} using 5 mg PS50PolyFR and the (d-f) corresponding profiles obtained at 10 K•min^{-1} using 10 mg PS50PolyFR.

both heating rates were conducted with 64 scans per spectrum, corresponding to acquisition intervals of 13 s. At 100 K•min^{-1}, this results in a lower number of data points across the HBr evolution profile, reducing the resolution of the integrated signal and contributing to the lower apparent HBr yield.

In addition, the maximum HBr absorbance at 100 K•min^{-1} marginally exceeds the calibrated upper limit of 0.071 (see Fig. 3). Maintaining absorbance values within the linear calibration range of the Beer-Lambert law is essential for accurate quantification. Under the applied conditions, particularly the high heating rate (100 K•min^{-1}) combined with a constant sample mass across experiments (5 or 10 mg), a rapid increase in HBr concentration occurs over a short time interval in the FTIR cell. As a result, a single data point at the peak of the HBr evolution profile slightly exceeds the calibrated range, while all other data points

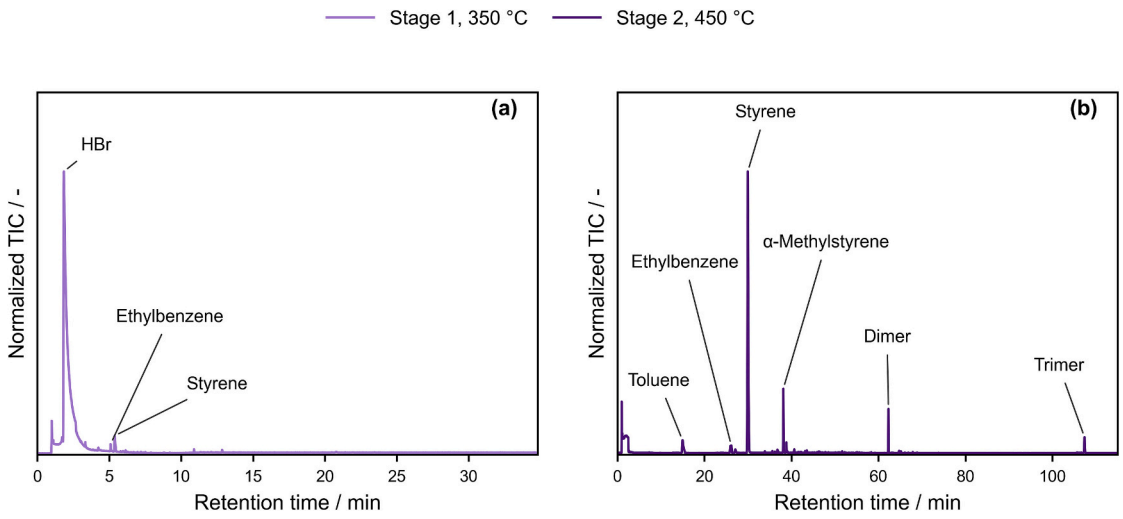

Fig. 12. Py-GC–MS chromatograms obtained during staged heating of PolyFR at (a) 350 °C and (b) 450 °C.

used for integration remain within it. This increases analytical uncertainty and may lead to an underestimation of the HBr yield. The results at 100 K•min^{-1} are therefore interpreted with caution. The analysis assumes that the volumetric contribution of pyrolysis volatiles to the total gas flow is negligible relative to the constant nitrogen purge, allowing a linear relationship between absorbance and HBr concentration. At 100 K•min^{-1}, the volumetric contribution of HBr between 250 and 275 °C remains below 0.2% of the total flow and is therefore considered negligible, indicating that dilution effects do not significantly influence HBr quantification. Despite these limitations, the results demonstrate rapid and substantial bromine release as HBr at heating rates relevant to technical pyrolysis.

The comparison between results obtained at 10 and 100 K•min^{-1} highlights opportunities for process design. In practice, bromine release as HBr can be achieved either through single-step pyrolysis at high heating rates or by deliberately exploiting the temperature-dependent separation between HBr release and PS decomposition observed at 10 K•min^{-1}. The latter enables staged pyrolysis concepts, in which bromine release is decoupled from PS depolymerization. To demonstrate this principle, temperature-staged pyrolysis of PolyFR was investigated using the micropyrolyzer, with a first stage at 350 °C followed by a second stage at 450 °C, as explained in Section 3.4. The resulting product spectra in Fig. 12 show that HBr is detected exclusively during the first stage at 350 °C, while no HBr or other brominated species are identified at 450 °C.

As staged pyrolysis was demonstrated only for PolyFR, further investigation is required to validate whether a comparable separation can be achieved in PS-PolyFR systems. Nonetheless, this initial analysis, supported by TG-FTIR results for both pure PolyFR and PolyFR-containing PS mixtures, demonstrates the technical feasibility of selectively separating HBr at temperatures below those require for PS decomposition.

4. Conclusion

This study demonstrates that pyrolysis enables effective separation of bromine from flame-retarded PS while preserving the formation of valuable styrene-rich hydrocarbon products, supporting its potential as a chemical recycling route for EPS from ETICS. At application-relevant flame-retardant loadings, neither HBCD nor PolyFR significantly alters the styrene-dominated product distribution. The effect of BFRs on styrene was evaluated semi-quantitatively, thus conclusions are based on relative peak areas. Future work should include quantitative calibration to assess styrene yield and its dependence on BFR presence more precisely.

Quantitative TG-FTIR analysis shows that approximately 90 wt% of bromine is released as HBr during the first decomposition step (≤350 °C), independent of PS-PolyFR mixture composition, indicating composition-independent dehydrobromination pathways. At higher temperatures (>372 °C), deviations from superposition behavior and delayed volatilization indicate interactions between PolyFR decomposition intermediates and PS, leading to stabilization effects and increased residue formation. A direct comparison with HBCD at elevated loadings is limited by regulatory restrictions. Hence, mechanistic insights for HBCD-PS interactions are inferred from literature.

The temporal separation between HBr release and hydrocarbon formation provides key insights for process design. High heating rates (100 K•min^{-1}) show rapid bromine release under conditions relevant to technical pyrolysis, while lower heating rates (10 K•min^{-1}) highlight the feasibility of selectively separating HBr evolution from hydrocarbon formation. Together, these results indicate that both single-step and temperature-staged pyrolysis are viable strategies for flame-retarded EPS.

For practical implementation, further investigation of real ETICS waste streams is required, particularly regarding inorganic constituents such as cement and mineral fillers, which may promote bromine retention in the solid fraction. In addition, the potential influence of molecular weight and its distribution on pyrolysis behavior should be assessed. Integration with downstream gas treatment and oil upgrading will be essential to meet the purity requirements for circular PS production. The substantial separation of bromine as HBr demonstrated in this study is expected to significantly reduce the burden on downstream purification, thereby supporting the development of scalable recycling strategies for flame-retarded PS waste.

CRediT authorship contribution statement

Razan Alsharqawi: Writing – review & editing, Writing – original draft, Visualization, Methodology, Investigation, Formal analysis, Data curation, Conceptualization. **Daniela Merz:** Writing – review & editing, Supervision, Resources, Methodology, Conceptualization. **Tim Kurtz:** Writing – review & editing, Resources, Methodology, Investigation. **Michael Zeller:** Writing – review & editing, Methodology. **Niklas Netsch:** Writing – review & editing, Methodology. **Britta Bergfeldt:** Writing – review & editing, Resources. **Salar Tavakkol:** Writing – review & editing, Supervision. **Dieter Stapf:** Writing – review & editing, Supervision, Funding acquisition.

Declaration of Generative AI and AI-assisted technologies in the writing process

In the course of preparing this work, the author used the tools "ChatGPT" by OpenAI and "DeepL" by DeepL SE to check grammar and spelling, and assist with improving English phrasing. "Semantic Scholar" by Allen Institute for AI and "Consensus" by Consensus AI were used to support literature search. All outputs generated with these tools were carefully reviewed and edited by the author, who takes full responsibility for the content of the publication.

Declaration of competing interest

The authors declare that they have no known competing financial interests or personal relationships that could have appeared to influence the work reported in this paper.

Acknowledgement

The authors thank LANXESS AG for providing the samples and funding this work. The authors gratefully acknowledge the additional funding provided by the Helmholtz Association within the program "Materials and Technologies for the Energy Transition". The authors also thank Iuliia Neugber and Aylin Hannemann for their support in samples preparation, as well as Lucas Bünger and Max Kleinebrahm for their efforts in reviewing this manuscript.

Appendix A. Supplementary data

Supplementary data to this article can be found online at https://doi.org/10.1016/j.cej.2026.177409.

Data availability

Data will be made available on request.

References

[1] European Union, Regulation (EU) 2019/1021 of the European Parliament and of the Council. https://eur-lex.europa.eu/eli/reg/2019/1021/oj, 2019 accessed June 26, 2025.
[2] European Union, A new Circular Economy Action Plan For A Cleaner and More Competitive Europe. https://eur-lex.europa.eu/legal-content/EN/TXT/?uri=celex:52020DC0098, 2020 accessed June 26, 2025.
[3] J. Schleier, G. Walther, Strategic network design for recycling of EPS insulation material – insights from a German case study, Int. J. Prod. Res. 62 (2024) 5878–5904, https://doi.org/10.1080/00207543.2024.2302041.
[4] Conversio Market & Strategy GmbH, EPS-Stoffstromanalyse Deutschland 2021. EPSStoffstromprognose ab 2022. Aufkommen und Management von EPSAbfällen aus dem Baubereich. https://www.ivh.de/wp-content/uploads/2024-11-28_Conversio_IVH_EPS-Stoffstroeme_Recyclingerlaeuterungen.pdf, 2023 accessed March 16, 2025.
[5] R. Bischof, R. Volk, F. Schultmann, Future disposal surge: a new quantification approach for predicting waste from external thermal insulation composite systems in Germany, J. Ind. Ecol. (2025) jiec.13624, https://doi.org/10.1111/jiec.13624.
[6] O. Dogu, M. Pelucchi, R. Van De Vijver, P.H.M. Van Steenberge, D.R. D'hooge, A. Cuoci, M. Mehl, A. Frassoldati, T. Faravelli, K.M. Van Geem, The chemistry of chemical recycling of solid plastic waste via pyrolysis and gasification: state-of-the-art, challenges, and future directions, Prog. Energy Combust. Sci. 84 (2021) 100901, https://doi.org/10.1016/j.pecs.2020.100901.
[7] F. Barontini, V. Cozzani, L. Petarca, Thermal stability and decomposition products of hexabromocyclododecane, Ind. Eng. Chem. Res. 40 (2001), https://doi.org/10.1021/ie001002v.
[8] M.A.E. Abdallah, M. Sharkey, H. Berresheim, S. Harrad, Hexabromocyclododecane in polystyrene packaging: a downside of recycling? Chemosphere 199 (2018) 612–616, https://doi.org/10.1016/j.chemosphere.2018.02.084.
[9] D. Jeannerat, M. Pupier, S. Schweizer, Y.N. Mitrev, P. Favreau, M. Kohler, Discrimination of hexabromocyclododecane from new polymeric brominated flame retardant in polystyrene foam by nuclear magnetic resonance, Chemosphere 144 (2016) 1391–1397, https://doi.org/10.1016/j.chemosphere.2015.10.021.
[10] A. Haarman, F. Magalini, J. Courtois, Study on the Impacts of Brominated Flame Retardants on the Recycling of WEEE plastics in Europe, 2020.
[11] Y. Wang, H. Jiang, J. Ni, J. Chen, H. Zhou, X. Wang, F. Xin, Study on the effect of PolyFR and its FR system on the flame retardancy and foaming behavior of polystyrene, RSC Adv. 9 (2019) 192–205, https://doi.org/10.1039/C8RA09680E.
[12] M.W. Beach, J.W. Hull, B.A. King, I.I. Beulich, B.G. Stobby, S.L. Kram, D. B. Gorman, Development of a new class of brominated polymeric flame retardants based on copolymers of styrene and polybutadiene, Polym. Degrad. Stab. 135 (2017) 99–110, https://doi.org/10.1016/j.polymdegradstab.2016.11.008.
[13] LANXESS Deuschland GmbH, LANXESS Bromine Solutions – Flame retardants product guide. https://www.biesterfeld.com/fileadmin/documents/product/Flame_Retardants_product_guide_04-2017.pdf, 2017.
[14] M. Schlummer, J. Vogelsang, D. Fiedler, L. Gruber, G. Wolz, Rapid identification of polystyrene foam wastes containing hexabromocyclododecane or its alternative polymeric brominated flame retardant by X-ray fluorescence spectroscopy, Waste Manag. Res. 33 (2015) 662–670, https://doi.org/10.1177/0734242X15589783.
[15] C. Koch, B. Sures, Degradation of brominated polymeric flame retardants and effects of generated decomposition products, Chemosphere 227 (2019) 329–333, https://doi.org/10.1016/j.chemosphere.2019.04.052.
[16] M.W. Beach, K.L. Kearns, J.W. Davis, J.R. Stutzman, D. Lee, Y. Lai, D. Monaenkova, S. Kram, J. Hu, C. Lukas, Stability assessment of a polymeric brominated flame retardant in polystyrene foams under application-relevant conditions, Environ. Sci. Technol. 55 (2021) 3050–3058, https://doi.org/10.1021/acs.est.0c04325.
[17] US EPA, Flame Retardant Alternatives for Hexabromocyclododecane (HBCD). https://www.epa.gov/sites/production/files/2014-06/documents/hbcd_report.pdf, 2014 accessed April 28, 2026.
[18] H. Knutsen, H.P.H. Arp, Preventing brominated flame retardants from occurring in recycled expanded polystyrene: comparing Norwegian visual sorting with advanced screening methods, J. Hazard. Mater. Lett. 2 (2021) 100016, https://doi.org/10.1016/j.hazl.2021.100016.
[19] L. Minet, A. Blum, S.R. Fernández, K.M. Rodgers, V. Singla, A. Soehl, M. L. Diamond, High production, low information: we need to know more about polymeric flame retardants, Environ. Sci. Technol. 55 (2021) 3467–3469, https://doi.org/10.1021/acs.est.0c08126.
[20] M. Holtkamp, M. Renner, K. Matthiesen, M. Wald, G.A. Luinstra, P. Biessey, Robust downstream technologies in polystyrene waste pyrolysis: design and prospective life-cycle assessment of pyrolysis oil reintegration pathways, Resour. Conserv. Recycl. 205 (2024) 107558, https://doi.org/10.1016/j.resconrec.2024.107558.
[21] W. Zhang, L. Cheng, R. Chen, J. Gu, J. Zheng, H. Yuan, Y. Chen, Millisecond dwell time enables closed-loop recycling of polypropylene waste plastics: effects of pyrolysis parameters on low-carbon olefin and carbon nanosphere formation, Chem. Eng. J. 517 (2025) 164273, https://doi.org/10.1016/j.cej.2025.164273.
[22] M. Zhang, Y. Zhang, D. Ma, A. Li, W. Fu, G. Ji, J. Dong, Numerical investigation on the heat transfer of plastic waste pyrolysis in a rotary furnace, Chem. Eng. J. 445 (2022) 136686, https://doi.org/10.1016/j.cej.2022.136686.
[23] B. Goshayeshi, R. Kumar, Y. Wang, R.J. Varghese, S. Roy, B. Baruah, A. A. Lemonidou, K.M. Van Geem, Enhancing polystyrene recycling: temperature-responsive of pyrolysis in a pilot-scale vortex reactor, J. Anal. Appl. Pyrolysis 187 (2025) 107016, https://doi.org/10.1016/j.jaap.2025.107016.
[24] L. Yao, X. Liu, Z. Song, Z. Wang, Y. Pang, S. Li, C. Huang, Microwave-assisted Fe-based catalytic conversion of plastic waste to hydrogen: ReaxFF-MD and DFT insights, Chem. Eng. J. 520 (2025) 166127, https://doi.org/10.1016/j.cej.2025.166127.
[25] J. Kaspersma, C. Doumen, S. Munro, A.-M. Prins, Fire retardant mechanism of aliphatic bromine compounds in polystyrene and polypropylene, Polym. Degrad. Stab. 77 (2002) 325–331, https://doi.org/10.1016/S0141-3910(02)00067-8.
[26] T.M. Kruse, O.S. Woo, H.-W. Wong, S.S. Khan, L.J. Broadbelt, Mechanistic modeling of polymer degradation: a comprehensive study of polystyrene, Macromolecules 35 (2002) 7830–7844, https://doi.org/10.1021/ma020490a.
[27] J. Zhou, Y. Qiao, W. Wang, E. Leng, J. Huang, Y. Yu, M. Xu, Formation of styrene monomer, dimer and trimer in the primary volatiles produced from polystyrene pyrolysis in a wire-mesh reactor, Fuel 182 (2016) 333–339, https://doi.org/10.1016/j.fuel.2016.05.123.
[28] Y. Ha, J. Jeon, Thermogravimetric analysis and pyrolysis characterization of expanded–polystyrene and polyurethane–foam insulation materials, Case Stud. Therm. Eng. 54 (2024) 104002, https://doi.org/10.1016/j.csite.2024.104002.
[29] A. Inayat, A. Fasolini, F. Basile, D. Fridrichova, P. Lestinsky, Chemical recycling of waste polystyrene by thermo-catalytic pyrolysis: a description for different feedstocks, catalysts and operation modes, Polym. Degrad. Stab. 201 (2022) 109981, https://doi.org/10.1016/j.polymdegradstab.2022.109981.
[30] M. Kusenberg, A. Eschenbacher, M.R. Djokic, A. Zayoud, K. Ragaert, S. Meester, K. M. Van Geem, Opportunities and challenges for the application of post-consumer plastic waste pyrolysis oils as steam cracker feedstocks: to decontaminate or not to decontaminate? Waste Manag. 138 (2022) 83–115, https://doi.org/10.1016/j.wasman.2021.11.009.
[31] P. Biessey, J. Vogel, M. Seitz, P. Quicker, Plastic waste utilization via chemical recycling: approaches, limitations, and the challenges ahead, Chem. Ing. Tech. 95 (2023) 1199–1214, https://doi.org/10.1002/cite.202300042.
[32] M.W. Beach, N.G. Rondan, R.D. Froese, B.B. Gerhart, J.G. Green, B.G. Stobby, A. G. Shmakov, V.M. Shvartsberg, O.P. Korobeinichev, Studies of degradation enhancement of polystyrene by flame retardant additives, Polym. Degrad. Stab. 93 (2008) 1664–1673, https://doi.org/10.1016/j.polymdegradstab.2008.06.010.
[33] M. Altarawneh, A. Saeed, M. Al-Harahsheh, B.Z. Dlugogorski, Thermal decomposition of brominated flame retardants (BFRs): Products and mechanisms, Prog. Energy Combust. Sci. 70 (2019) 212–259, https://doi.org/10.1016/j.pecs.2018.10.004.

[34] E.R. Larsen, E.L. Ecker, Thermal stability of fire retardants: I, hexabromocyclododecane (HBCD), J. Fire Sci. 4 (1986) 261–275, https://doi.org/10.1177/073490418600400403.
[35] K. Grönlund, V.H. Nissinen, I. Rytöluoto, M. Mosallaei, J. Mikkonen, K. Korpijärvi, P. Auvinen, M. Suvanto, J.J. Saarinen, J. Jänis, Direct mass spectrometric analysis of brominated flame retardants in synthetic polymers, ACS Omega (2024) acsomega.4c04059, https://doi.org/10.1021/acsomega.4c04059.
[36] V.H. Nissinen, K. Grönlund, N. Heilala, I. Rytöluoto, M. Mosallaei, K. Korpijärvi, P. Auvinen, M. Suvanto, J.J. Saarinen, J. Jänis, Quantification of brominated flame retardants in synthetic polymers via direct mass spectrometric analysis, Anal. Chem. 97 (2025) 8600–8608, https://doi.org/10.1021/acs.analchem.5c00946.
[37] INEOS Styrolution, Styrolution PS 124N/L Technical Datasheet. https://eshop.ineos-styrolution.com/INTERSHOP/web/WFS/Styrolution-Portal-Site/en_US/-/USD/ViewPDF-Print.pdf?SKU=200300060569&RenderPageType=ProductDetail, 2022 accessed April 22, 2026.
[38] N. Netsch, L. Schröder, M. Zeller, I. Neugber, D. Merz, C.O. Klein, S. Tavakkol, D. Stapf, Thermogravimetric study on thermal degradation kinetics and polymer interactions in mixed thermoplastics, J. Therm. Anal. Calorim. (2025), https://doi.org/10.1007/s10973-024-13630-6.
[39] M. Zeller, K. Garbev, L. Weigel, T. Saatzer, D. Merz, S. Tavakkol, D. Stapf, Thermogravimetric studies, kinetic modeling and product analysis of the pyrolysis of model polymers for technical polyurethane applications, J. Anal. Appl. Pyrolysis 171 (2023) 105976, https://doi.org/10.1016/j.jaap.2023.105976.
[40] D.A. Schindler, Average Curve and SuperPosition of Curves, (n.d.). https://analyzing-testing.netzsch.com/_Resources/Persistent/c/1/d/7/c1d7e3c2596336bfc2c52b754a8cf65ca395955c/Software%20Innovation%20005_EN.pdf.
[41] A.I. Balabanovich, A. Hornung, D. Merz, H. Seifert, The effect of a curing agent on the thermal degradation of fire retardant brominated epoxy resins, Polym. Degrad. Stab. 85 (2004) 713–723, https://doi.org/10.1016/j.polymdegradstab.2004.02.012.
[42] D. Merz, O. Dregert, J. Vehlow, High resolution as solution - TA-HR-FTIR for highly complex samples, in: E. Kapsch (Ed.), Hyphenated Tech. Therm. Anal, 2003, pp. 69–82, n.d. https://www.degruyterbrill.com/document/doi/10.1524/9783486593938.69/html.
[43] M. Zeller, D. Merz, L. Weigel, S. Tavakkol, D. Stapf, TG-FTIR investigations of the pyrolysis of polyurethanes: quantitative carbon dioxide tracing, decomposition mechanisms, products and mass balances for advanced recycling, J. Anal. Appl. Pyrolysis 188 (2025) 107048, https://doi.org/10.1016/j.jaap.2025.107048.
[44] M.M. Koek, R.H. Jellema, J. Van Der Greef, A.C. Tas, T. Hankemeier, Quantitative metabolomics based on gas chromatography mass spectrometry: status and perspectives, Metabolomics 7 (2011) 307–328, https://doi.org/10.1007/s11306-010-0254-3.
[45] Y. Liu, A. Ali Siyal, C. Zhou, C. Liu, J. Fu, Y. Zhang, B. Yao, L. Chao, H. Yun, J. Dai, X. Bi, Microwave co-pyrolysis of industrial sludge and waste biomass: product valorization and synergistic mechanisms, Chem. Eng. J. 485 (2024) 150032, https://doi.org/10.1016/j.cej.2024.150032.
[46] J. Huang, H. Meng, G. Pan, S. Wang, D. Wang, Density functional theory study on the catalytic degradation mechanism of polystyrene, AIP Adv. 10 (2020) 085004, https://doi.org/10.1063/5.0013211.
[47] X. Ni, L. Wu, Enhanced flame retardancy and thermal stability in flexible polyurethane foam through synergistic core-shell structured DBDPE@PMA particles, Arab. J. Chem. 17 (2024) 105684, https://doi.org/10.1016/j.arabjc.2024.105684.
[48] T. Faravelli, M. Pinciroli, F. Pisano, G. Bozzano, M. Dente, E. Ranzi, Thermal degradation of polystyrene, J. Anal. Appl. Pyrolysis (2001) 103–121.
[49] Hydrogen bromide, NIST Chem. WebBook SRD 69 (n.d.). https://webbook.nist.gov/cgi/cbook.cgi?ID=C10035106&Mask=200#Mass-Spec (accessed August 12, 2025).
[50] J.J. Brocks, J.M. Hope, Tailing of chromatographic peaks in GC-MS caused by interaction of halogenated solvents with the ion source, J. Chromatogr. Sci. 52 (2014) 471–475, https://doi.org/10.1093/chromsci/bmt068.
[51] J. Tae, Catalytic degradation of polystyrene using acid-treated halloysite clays, Solid State Ionics 172 (2004) 129–133, https://doi.org/10.1016/j.ssi.2004.05.013.
[52] B. Dodson, I.C. McNeill, Degradation of polymer mixtures. VI. Blends of poly(vinyl chloride) with polystyrene, J. Polym. Sci. 14 (1976) 353–364, https://doi.org/10.1002/pol.1976.170140208.
[53] G. Drefahl, H.-H. Hörhold, E. Hesse, Umwandlung von *cis* - und *trans* -1,4-polybutadien in polymere mit konjugierten doppelbindungssystemen, J. Polym. Sci. Part C Polym. Symp. 16 (1967) 965–970, https://doi.org/10.1002/polc.5070160231.
[54] H. Oumeddour, H. Aldoori, Z. Bouberka, V.R. Mundlapati, V. Madhur, C. Foissac, P. Supiot, Y. Carpentier, M. Ziskind, C. Focsa, U. Maschke, Degradation processes of brominated flame retardants dispersed in high impact polystyrene under UV–visible radiation, Waste Management & Research 42 (2024) 1241–1252, https://doi.org/10.1177/0734242X231219626.